Synergistic Role of Sodium Hydroxide and Sodium Citrate on Bitumen Slime Coating in Process Water

by

Zhiqing Zhang

A thesis submitted in partial fulfillment of the requirements for the degree of

Master of Science

in

Chemical Engineering

Department of Chemical and Materials Engineering
University of Alberta

Abstract

Sodium hydroxide (NaOH) is generally used as the primary processing aid in the water-based oil sands extraction for the recovery of bitumen. It was found by Syncrude Canada Ltd. that the combined use of sodium hydroxide and sodium citrate could effectively improve the bitumen recovery as compared to using sodium hydroxide alone. Thus, sodium citrate is introduced as a secondary process aid (SPA) in the water-based extraction.

Slime coating in the bitumen extraction is the attachment of undesired clay particles onto bitumen, thereby reducing bitumen recovery and froth quality. It is believed that the addition of sodium citrate prevents the hetero-coagulation of bitumen droplets and clay particles, enhancing the bitumen recovery. Moreover, the combined use of sodium hydroxide and sodium citrate is believed to further prevent bitumen-clay coagulation by their synergistic effect. In this research, the synergistic role of sodium hydroxide and sodium citrate on preventing slime coating of bitumen with various clay particles were investigated using process water.

Adding sodium citrate was able to make the zeta potential of kaolinite, illite, montmorillonite, and bitumen more negative in the process water. The zeta potential of the mixture of bitumen with non-swelling clays (kaolinite and illite) showed two separated distributions in the process water, suggesting that no slime coating had happened. However, single distribution of zeta potential of bitumen-montmorillonite mixture was observed in process water. The addition of sodium citrate before mixing bitumen and montmorillonite could effectively prevent slime coating. Results obtained from zeta potential distribution measurements were verified by Quartz Crystal Microbalance with Dissipation (QCM-D), and consistent results were observed.

Sodium citrate alone could not change the zeta potential of real fines in the process water, but it could work synergistically with sodium hydroxide to change the zeta potential of real fines. For

the mixture of bitumen and fines, experimental results showed that the consequent effect of more negatively charged colloidal particles (bitumen and fines) due to the combined use of sodium hydroxide and sodium citrate prevented the hetero-coagulation of bitumen and real fines.

Acknowledgements

First, I would like to be sincerely grateful to my supervisor Professor Qingxia Liu, for his kind support, scientific training, and patient guidance during my MSc program. He provided me valuable study and research opportunities, as well as advanced scientific research environment and equipment. The knowledge I gained and the research skills I mastered bring good preparation for my future.

I would like to express my special gratitude to Dr. Jun Long, for providing research project and funding, experimental materials, and great suggestions.

I want to thank Dr. Rogerio Manica, Dr. Yi Lu, Dr. James Grundy, Dr. Bo Liu, and Dr. Bailin Xiang for lots of discussions on scientific topics, my research project, experiments, and academic writing. I could not make much progress without their help.

I want to thank James Skwarok, Liyuan Feng, Hanrui Zheng, Mingda Li, and Caroline da Costa for their help on the equipment setup and training. I would also like to extend my appreciation to all of secondary process aids team for their support and collaboration.

Financial support from Natural Sciences and Engineering Research Council of Canada (NSERC)/Syncrude CRD project is highly appreciated.

Finally, my deepest gratitude goes to my parents for their love and support in my life.

Table of Contents

List of Figures

List of Tables

Chapter 1 Introduction

1.1. Background

Canada has abundant oil sands deposits, mainly located in Athabasca, Cold Lake, and Peace River. Oil sands extraction contains few sub-steps such as bitumen liberation, bitumen aeration, flotation, and water management. The liberated bitumen interacts with various colloidal components such as bitumen droplets, air bubbles, and clays. Among them, interactions between bitumen and fines are detrimental. The attachment of fines on bitumen generates a steric barrier, which hinders the attachment between bitumen and air bubbles.

Sodium hydroxide (NaOH) is currently the most widely used processing aid in the oil sands extraction operation. It plays many roles in the whole extraction process. For example, it leads to the negatively charged bitumen and solid surfaces, thereby promoting electrostatic repulsive forces (Liu, Xu, & Masliyah, 2003). NaOH hydrolyzes the solid surface, rendering the solid hydrophilic, facilitating liberation and reducing the attachment of bitumen and fine solids (Flury, Afacan, Tamiz Bakhtiari, Sjoblom, & Xu, 2014). In addition, the formation of calcium carbonate is promoted at high pH, which is helpful for reducing slime coating. However, the negatively charged surfaces of bitumen and air are not beneficial for aeration.

Syncrude Canada Ltd initiated a novel technology regarding bitumen extraction from mined oil sands. It relies on the combined use of sodium hydroxide and sodium citrate, in which sodium hydroxide is still used as the primary process aid with a little amount of sodium citrate used as secondary process aid. It was found from tests that the combined use of primary and secondary process aids improves bitumen recovery and froth quality, which is commercially promising. However, the fundamental understanding of the underlying mechanism of the role of secondary process aid still needs to be investigated.

1.2. Research Objectives

Previous studies by zetaphoremeter have shown that montmorillonite causes slime coating especially in the presence of divalent cations (Liu, Zhou, Xu, & Masliyah, 2002). A stronger adhesion force between bitumen and montmorillonite than that between bitumen and kaolinite was measured by Liu, Xu, & Masliyah (2005) in the presence of calcium. Force measurements were also conducted between bitumen and fines from good and poor ores. It was found that the adhesion force is stronger between bitumen and fines from poor ore due to the hydrophobic nature of fines (Liu, Xu, & Masliyah, 2004). Zhang (2020), using zetaphoremeter and QCM-D, showed that the addition of sodium citrate alone could prevent slime coating caused by montmorillonite. However, all previous research was performed in ideal systems such as ideal solution or purchased clay particles. The role of sodium citrate on slime coating in process water with real fines is still lacking. Additionally, the combination of sodium hydroxide and sodium citrate on the slime coating of bitumen and fine particles needs investigating.

This study aims to fundamentally understand, from ideal system to real system, the role of sodium citrate on the interactions of bitumen and clay particles, as well as investigating how sodium citrate works synergistically with sodium hydroxide to prevent slime coating from happening.

1.3. Thesis Outline

The structure of thesis is organized as follows:

Chapter 1:

Introduces the background and objectives of the research.

Chapter 2:

Reviews the basic water-based extraction of bitumen, the role of caustic addition, the effect of clays in the oilsands, and the issues caused by slime coating.

Chapter 3:

Presents the role of sodium citrate alone on the zeta potential of kaolinite, illite, montmorillonite, and bitumen in the process water from Aurora plant.

Uses Zetaphoremeter to measure the zeta potential distribution of the mixture of bitumen-kaolinite, bitumen-illite, and bitumen-montmorillonite in the presence or absence of sodium citrate.

Uses QCM-D to study the possible adsorption of kaolinite, illite, and montmorillonite at bitumen-water interface and investigate the effect of sodium citrate on these adsorptions.

Uses SEM to look at morphology of montmorillonite sticked on bitumen and EDS to analyze the map of element spectrum of clay.

Chapter 4:

Uses zeta potential distribution measurement to study the role of sodium citrate and the synergistic effect of sodium citrate on the zeta potential change of three different kinds of real fines obtained from oil sands industry.

Investigates the synergistic effect of sodium citrate and sodium hydroxide on preventing slime coating of real fines.

Links the relation between hydrophobicity of kaolinite and slime coating.

Chapter 5:

Concludes the research and proposes future work.

Chapter 2 Literature Review

2.1. Alberta Oil Sands

Oil sands, also referred as tar sands or bituminous sands, are composed of solids with different size, bitumen, and water (Masliyah, Czarnecki, & Xu, 2011). Bitumen content could range from zero to 16% by weight. Depending on the degree of weathering of the oil sands ore, water content could be zero if oilsands are dewatered and it could reach up to 7% by weight. It is hypothetically believed that there exists a thin layer of roughly 10 nm water film located between sands and bitumen in Alberta oil sands (Madge, Romero, & Strand, 2004) as shown in Figure 2.1, which provides processability and feasibility of water-based extraction. Clay minerals are believed to be suspended in the water phase of oil sands (Takamura, 1982). Sands are believed to be hydrophilic, which provide a solid basis that water based extraction operation works well for Alberta oil sands (Masliyah, Czarnecki, & Xu, 2011). For hydrophobic sand, bitumen is in direct contact with sand so that such oil sands cannot be processed such as Utah oil sands (Sepulveda and Miller 1978; Miller and Misra 1982; Misra and Miller 1991).

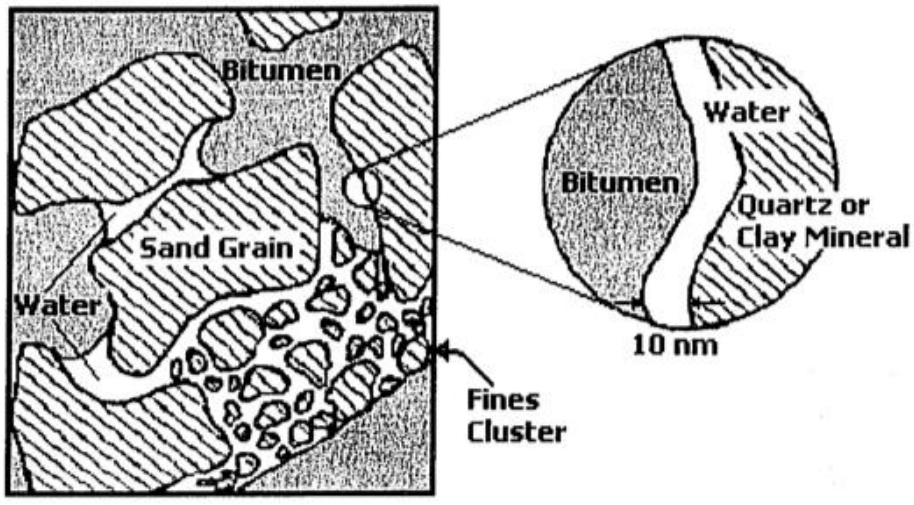

Figure 2.1. Model structure of Alberta oil sands (Madge, Romero, & Strand, 2004).

Bitumen is a form of petroleum, but it must be processed to transform to synthetic crude oil. The viscosity of bitumen is higher than 500 Pa·s at room temperature and the density of bitumen is comparable to water (Masliyah, Czarnecki, & Xu, 2011).

2.2. Industrial Process

Two industrial methods generally used to recover bitumen from Athabasca oil sands are open-pit mining and steam-assisted gravity drainage (SAGD) (Masliyah, Czarnecki, & Xu, 2011). The limitation of operation methods is based on the overburden thickness that open-pit mining is usually employed where overburden thickness is less than ~75 m. Open-pit mining uses truck-and-shovel to mine oil sands ore and the mined oil sands are further processed with hot water to recover bitumen. Open-pit mining operations requires 7% by weight of bitumen in oil sands to be the cut-off for mining because there is less commercial value to process oil sands with low grade. SAGD method uses two vertical parallel pipelines to extract bitumen. Hot steam is introduced into the upper pipeline to heat the surrounding oil sands ores. The bitumen viscosity is thus reduced, and bitumen could flow downwards to the lower pipeline and be pumped to the ground.

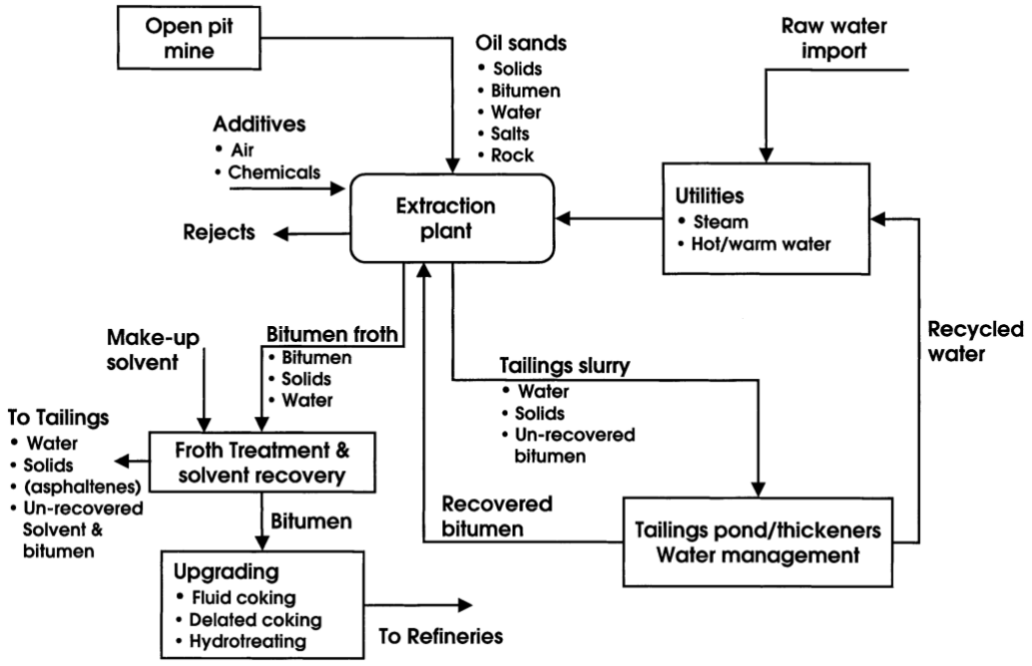

Figure 2.2. Industrial process of water-based bitumen extraction (Masliyah et al., 2004)

Hot water-based bitumen extraction was first applied by Clark (Clark & Pasternack, 1932), and it has been the basis of current widely used water-based bitumen extraction (Masliyah et al., 2004). The operation temperature of hot water-based bitumen extraction is usually around 80 °C (Clark & Pasternack, 1932). Currently, warm water around 40-55 °C has been successfully used in water-based bitumen extraction instead of hot water (Long, Drelich, Xu, & Masliyah, 2007). As indicated in Figure 2.2, typical water-based bitumen extraction process comprises slurry preparation, hydrotransport, extraction, froth treatment, tailing, and water management. Oil sands, which are mined at open-pit mine and crushed, are mixed with recycled process water and chemical additives in the slurry preparation to reduce the size of oil sand ores. Hydrotransport is the following step where the size of oil sands in the prepared slurry is further reduced, and bitumen is liberated from the sand. Meanwhile, air bubbles are introduced and attach to the liberated bitumen.

Later, diluted slurry is transported into the primary separation vessel (PSV) within the extraction plant, where aerated bitumen float to the top to become froth, coarse solids settle to the bottom, and fine solids are suspended in the middle. Froth collected normally contains 60% bitumen, 30% water, and 10% solids (Masliyah, Czarnecki, & Xu, 2011). Froth is diluted by solvent to reduce the viscosity and density of bitumen. The bitumen is then separated from water and solids, referred as froth treatment. Bitumen collected from froth treatment is sent to upgrading. The settled parts in the separation vessel become tailing slurries and are introduced to either thickeners or tailing ponds where water is recycled.

2.2.1. Water-based Extraction

The overall process of bitumen extraction consists of liberation, aeration, coalescence, and flotation (Masliyah, Zhou, Xu, Czarnecki, & Hamza, 2004). Normally, liberation is the primary step where recession of the bitumen thin film and detachment of bitumen droplets from sand happens. Bitumen film will first thins until it reaches a critical thickness that results in film rupture. Later, the three-phase contact line (TPCL) starts moving and the bitumen-sand interface is replaced by water-sand interface, and eventually bitumen is detached from sand. In the next step, liberated bitumen droplets collide with introduced air bubbles. The subsequent attachment of bitumen with air bubbles is defined as aeration. In the meantime, some small, liberated bitumen droplets coalesce to form larger ones. The coalescence increases the size of bitumen droplets and thereby increase bitumen recovery. Finally, the bitumen-bubble aggregates float to the top because of its sufficient buoyancy. Slime coating (more details are discussed in section 2.5) of bitumen by clays happens during the recovery process and reduces bitumen recovery.

2.2.2. Interfacial Energy

Interfacial energy plays an important role in bitumen liberation and aeration since the formation of interfaces between bitumen, sand, water, and air would be either thermodynamically favorable or unfavorable.

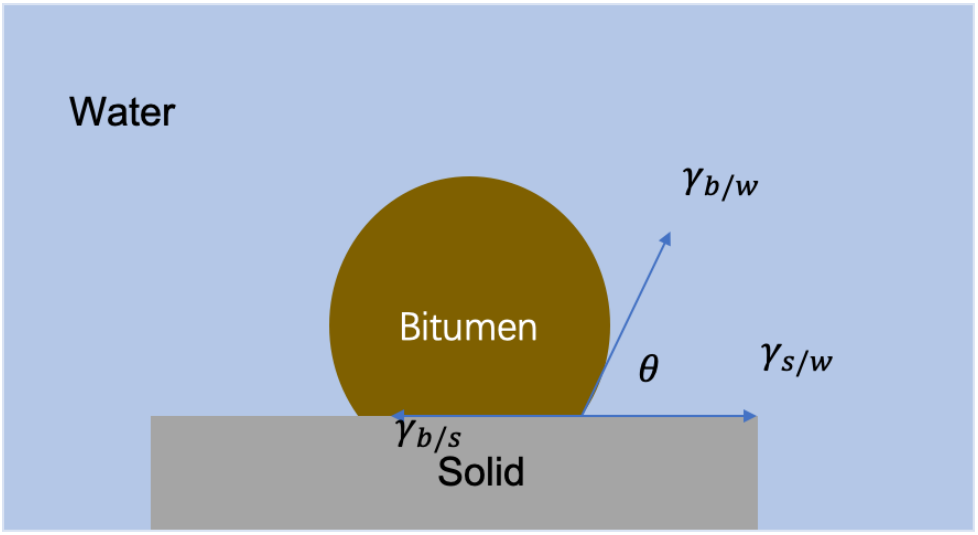

Figure 2.3. Interfacial energies in the bitumen-water-solid system.

Figure 2.3 shows energy changes related to bitumen recession where $\gamma_{b/s}$, $\gamma_{b/w}$, $\gamma_{s/w}$, and θ refer to interfacial free energy of bitumen-sand, bitumen-water, sand-water, and contact angle at the three-phase contact line, respectively. The interfacial energy change of sand-water interface displacing bitumen-sand interface is then given by

$$\frac{\Delta G}{\Delta A} = \gamma_{s/w} - \gamma_{b/s} \tag{2.1}$$

The above equation links the relationship of interfacial energy changes and interfacial tension during bitumen recession, but it is difficult to directly measure the interfacial tension of bitumen-sand and sand-water. Therefore, interfacial tension of bitumen-sand and sand-water are linked by Young's equation,

$$\gamma_{b/s} - \gamma_{s/w} = \gamma_{b/w} \cos\theta \tag{2.2}$$

Equations 2.1 and 2.2 could be rewritten as equation 2.3,

$$\frac{\Delta G}{\Delta A} = -\gamma_{b/w} \cos\theta \tag{2.3}$$

As shown in equation 2.3, the contact angle determines whether bitumen recession is energetically favorable or unfavorable. If the contact angle is smaller than 90° (hydrophilic sands), the left-hand side of equation 2.3 would be less than zero and bitumen recession is energetically favorable. On the contrary, if the contact angle is larger than 90° (hydrophobic sands), bitumen recession is energetically unfavorable. The contact angle is defined from the water side. From equation 2.3, it could be noted that smaller contact angle and larger bitumen-water interfacial tension are beneficial for bitumen recession.

Bitumen detachment happens until bitumen recedes to a critical shape. The interface between bitumen and sand would disappear and extra interfaces of bitumen-water and sand-water would be generated. This process could be described by equation 2.4,

$$\frac{\Delta G}{\Delta A} = \gamma_{s/w} + \gamma_{b/w} - \gamma_{b/s} \tag{2.4}$$

which could also be linked with Young's equation and rewritten as

$$\frac{\Delta G}{\Delta A} = \gamma_{b/w}(1 - \cos\theta) \tag{2.5}$$

The right-hand side of equation 2.5 would never be less than zero. Therefore, detachment of bitumen from sands is always thermodynamically unfavorable. From equation 2.5, it is noted that less bitumen-water interfacial tension is beneficial for bitumen detachment. Positive free energy should be as small as possible in order to facilitate bitumen detachment.

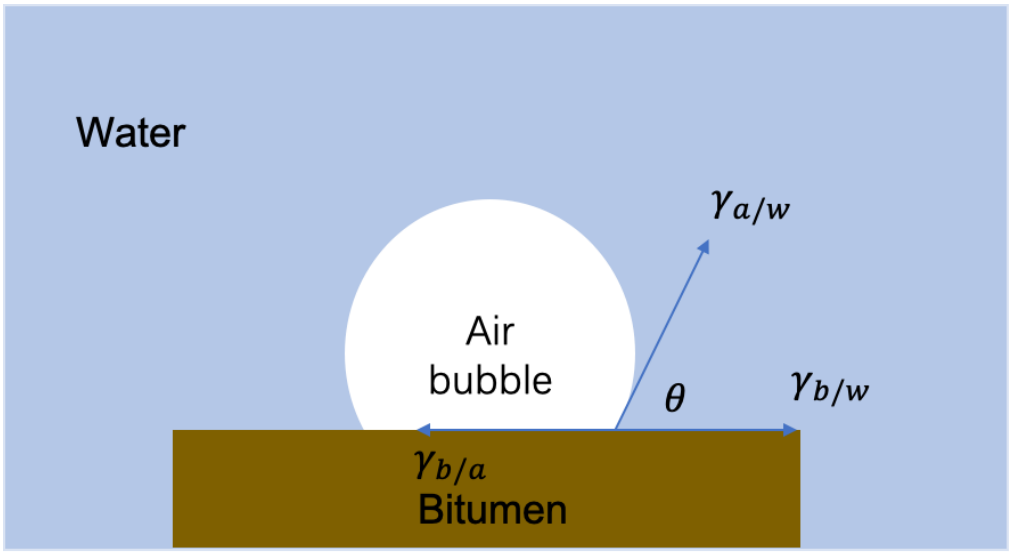

Figure 2.4. Interfacial energies in the bitumen-water-air system.

In the aeration step, interfacial energy is related to the generation of bitumen-air interface and the interfacial changes of bitumen-water and water-air could be described as

$$\frac{\Delta G}{\Delta A} = \gamma_{b/a} - (\gamma_{b/w} + \gamma_{a/w}) \tag{2.6}$$

where $\gamma_{b/a}$ and $\gamma_{a/w}$ indicate interfacial tension of bitumen-air and air-water, respectively. Equation 2.6 could be again inserted by Young's equation

$$\gamma_{b/a} - \gamma_{b/w} = \gamma_{a/w} \cos\theta \tag{2.7}$$

Then equation 2.7 leads to

$$\frac{\Delta G}{\Delta A} = \gamma_{a/w}(\cos\theta - 1) \tag{2.8}$$

It is very conclusive from equation 2.8 that for aeration process, interfacial energy is always negative so that air attaching to bitumen is energetically spontaneous.

2.3. Zeta Potential

There are few reasons of colloidal particles being charged when they are brought into solution such as hydrolysis of broken surface sites, ion adsorption, and isomorphic substitution of high valence cation by lower valence cation in clay (Sposito, 2019). Additionally, unequal dissolution of ions that form crystal lattice leads to surface charge (Schramm, Mannhardt, & Novosad, 1991). The charged solid-aqueous interface could attract counterions due to electrostatic interaction and form a layer, which is referred as Stern layer. However, not all charges could be balanced by attracted ions in the aqueous phase. Because of thermal fluctuations, counterions are driven to diffuse away from the surface and form a diffuse layer, which is more extended than the Stern layer. Thus, the formation of the Stern layer and diffuse layer are called the build-up of the electrical double layer. When a charged colloidal particle moves under the applied electric field, ions inside the Stern layer are relatively immobile to the particle and move together with the particle while ions inside the diffuse layer are mobile and do not move with the same velocity as the particle. Between the immobile layer of ions and the mobile layer of ions is the shear plane. Zeta potential is defined as the potential of the shear plane of moving colloidal particles under the electric field.

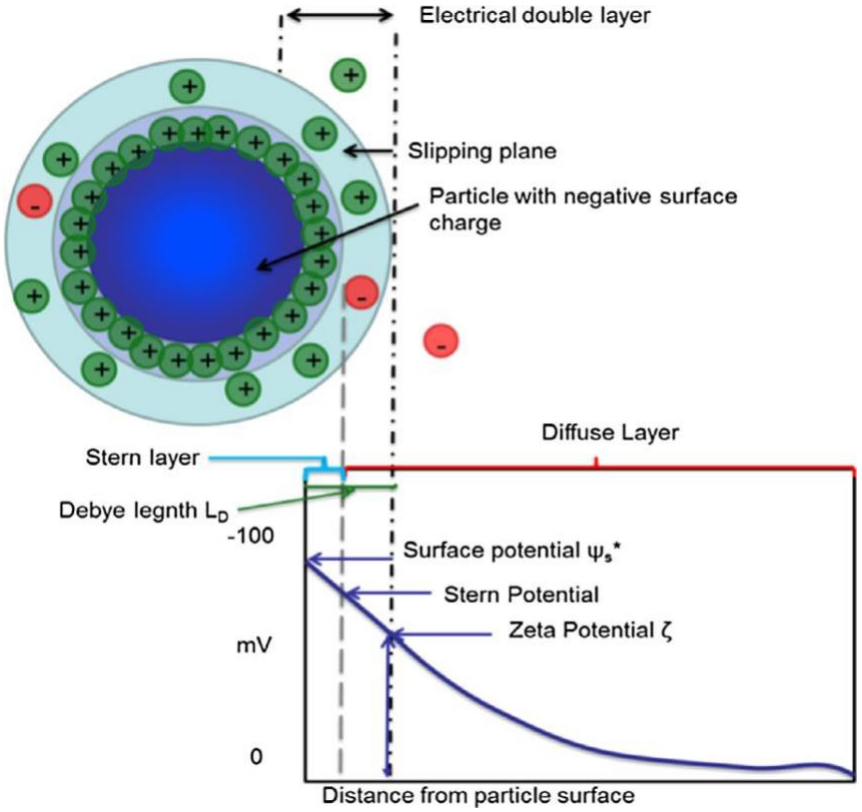

Figure 2.5. Electrical double layer structure around colloidal particle and potential distribution (Vali et al., 2014).

Potential distribution from the colloidal particle-aqueous interface to the bulk solution is shown in Figure 2.5. The potential decrease exponentially from the shear plane to the bulk, and the decay length is referred as Debye length. Electrolytes affect the zeta potential of colloidal particles by either specifically adsorbing at the solid-water interface or non-specific interaction. The latter contributes to the ionic strength and affects the electrical double layer thickness, thereby changing the magnitude of the zeta potential without changing the sign of the zeta potential. Normally, the magnitude decreases with increasing the ionic strength. However, specific adsorption results in charge reversal in some situations (Rabiller-Baudry & Chaufer, 2001). The specific adsorbed ions are believed to enter the Stern layer while non-specific ions stay in the

diffuse layer (Chang et al., 2021). Higher valence of cations was reported to be more strongly adsorbed on clay surfaces than lower valence of cations (Lagaly 2013).

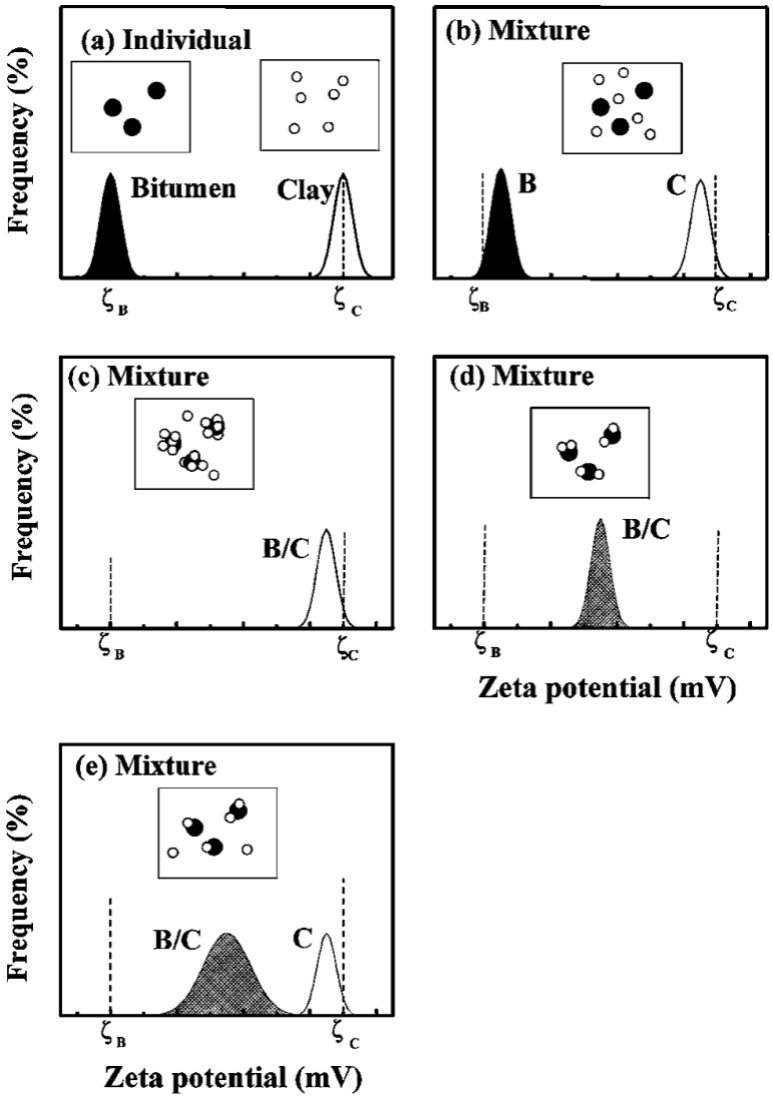

Figure 2.6. Schematic illustration for zeta potential distribution of binary system. Black and white circles indicate bitumen and clay that there might be interactions between them. (Liu et al., 2002).

Zeta potential distribution measurements has been used widely to study the interaction between binary colloidal systems, the systems investigated by this method are listed in Table 2.1.

For bitumen and clay, as shown in Figure 2.6, basic principle of this method is that two colloidal systems have different zeta potential distributions when they are measured individually. When the zeta potentials of their mixtures are measured, two separated distributions indicate no interactions between them, while single distribution suggests possible hetero-coagulation of these two colloidal types.

Table 2.1. Binary system studied by zeta potential distribution measurement

Binary Systems	References
Bitumen-Kaolinite	Liu, Xu, & Masliyah, 2004a
Bitumen-Illite	Ding et al., 2008
Bitumen-Montmorillonite	Liu et al., 2002
Bitumen-Fines	Liu, Xu, & Masliyah, 2004
Bitumen-Silica	Zhao et al., 2006
Silica-Bubble	Wu et al., 2015
Silica-Ceria Nanoparticles	Lin et al., 2012
Silica-Sphalerite	Deng, Liu, & Xu, 2013
Kaolinite-Chalcopyrite	Forbes, Davey, & Smith, 2014
Talc-Ink	Liu et al., 2007

2.4. Clays in Oil Sands

Clays in the oil sands cause slime coating on bitumen droplets and prevent bitumen aeration, reducing bitumen recovery. The bitumen in the water emulsion could be stabilized by clays in the froth treatment process and create problems for later upgrading. Clays also contribute to mature

fine tailings. Thus, clays play different roles in the whole bitumen extraction process, and it is of significance to understand properties of clays to face challenges caused by them.

The structure of clay is mainly composed of tetrahedron and octahedron sheets (Schoonheydt et al., 2018). In the tetrahedron sheet, silica atom coordinates with four surrounding oxygen atoms, in which three oxygen atoms bridge adjacent tetrahedron via sharing three corners. Such oxygen atoms form hexagonal mesh network on the basal plane of tetrahedron sheet. The side view and the top of clay minerals are illustrated in Figures 2.7 and 2.8. The fourth oxygen atom links to octahedron sheet.

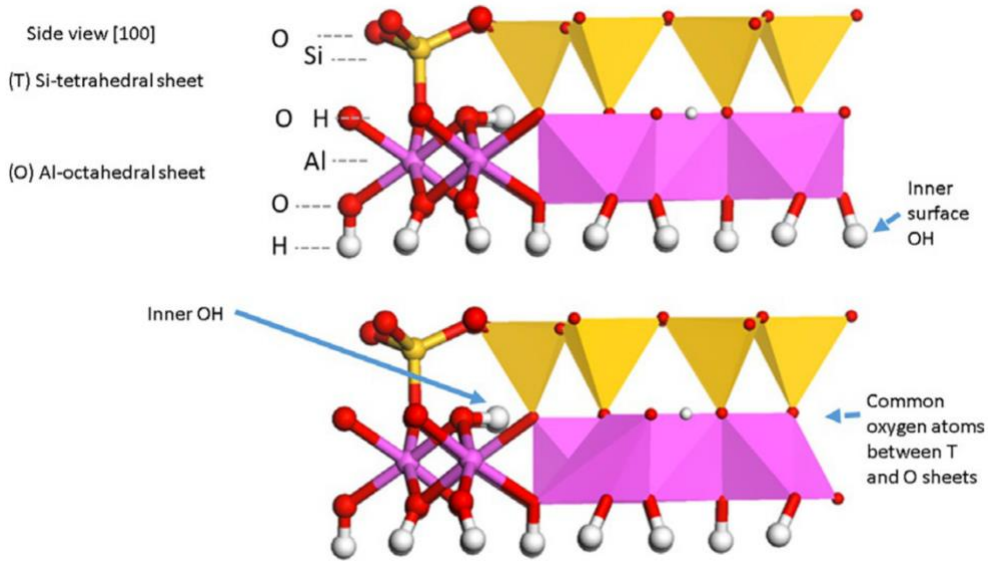

Figure 2.7. Side view of TO clay (Schoonheydt et al., 2018).

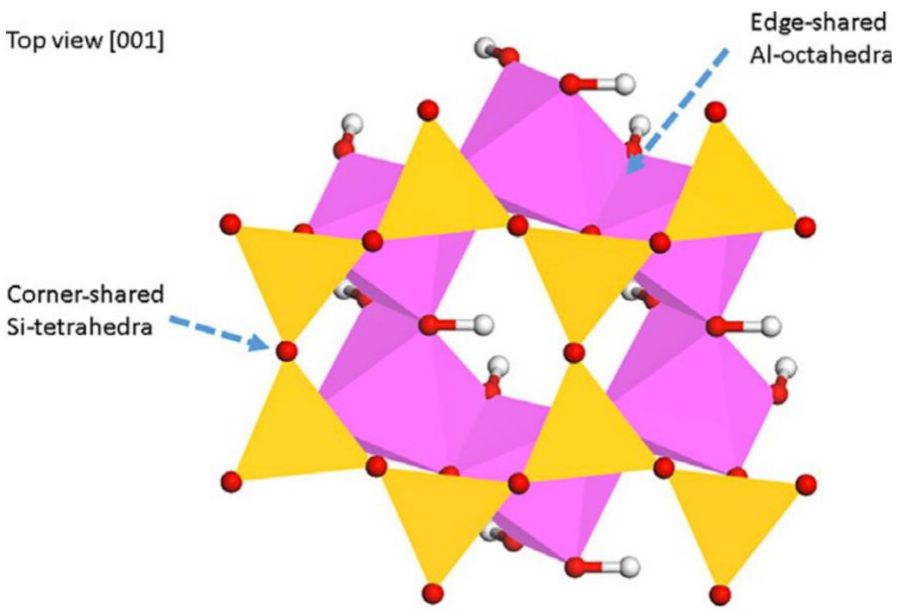

Figure 2.8. Top view of TO clay (Schoonheydt et al., 2018).

In the octahedron sheet, metal ions are either divalent cations such as Mg^{2+} or Fe^{2+} in which all octahedral sites are occupied by metal ions and result in tri-octahedron sheet, or trivalent ions such as Al^{3+} and Fe^{3+} in which two-thirds of octahedral sites are occupied by metal ions and result in di-octahedron sheet (Tournassat, Bourg, Steefel, & Bergaya, 2015). In 1:1 TO clay, one basal plane is totally composed of oxygen atoms belonging to tetrahedron sheet and the other basal plane is composed mostly of -OH group belonging to octahedron sheet. In 2:1 TOT clay, both basal planes are composed of oxygen atoms belonging to tetrahedron sheet and some of -OH groups are replaced by oxygen atoms that connect to octahedron sheet.

Isomorphic substitution is referred to the substitution of higher valence of metal ions by lower valence of metal ions in T-sheet or O-sheet or both and cause permanent layer charge (Mignon, Ugliengo, Sodupe, & Hernandez, 2010). The typical substitutions are Si^{4+} by Al^{3+} in tetrahedral sheet, Al^{3+} by Mg^{2+} in dioctahedral sheet, and Mg^{2+} by Li^{+} in trioctahedral sheet (Schoonheydt &

Johnston, 2006). Such charge unbalance results in charge compensation of alkali and alkaline metal ions such as Na^+, K^+, Ca^{2+}, and Mg^{2+} on the clay basal plane. The location of substitution of different kinds of three-layers clay varies and results in different behaviors in the processing of oil sands.

2.4.1. Kaolinite

Kaolinite is the most abundant clay in oil sands. It is composed of a layer of silicon-oxygen tetrahedron sheet and a layer of aluminum-oxygen-hydroxyl octahedron sheet (TO). Kaolinite unit layers are bonded by the hydrogen bond between oxygen in the basal plane of tetrahedron sheet and hydroxyl group in the basal plane of octahedron sheet (Benco, Tunega, Hafner, & Lischka, 2001). These hydrogen bonding connect kaolinite unites strongly so that kaolinite is non-swelling clay (Reddi & Inyang, 2000). Besides, the ions cannot go inside the interlayer of kaolinite due to hydrogen bonding and cations exchange is believed to be low. Another reason why kaolinite has low cation exchange capacity and is non-swelling is that compensating ions are located in the holes of hexagonal pattern and bind kaolinite units strongly (Bergaya, Theng, & Lagaly, 2006). The ideal structure of kaolinite was first outlined through modelling by (Pauling, 1930). The real structure of kaolinite was first reported by Gruner (1932) through XRD pattern.

The bimodal zeta potential of the mixture of kaolinite and bitumen in the presence of divalent cations were observed, concluding that there was marginal slime coating of bitumen by kaolinite (Liu, Zhou, Xu, & Masliyah, 2002). The weak adhesion force between kaolinite and bitumen surface in the presence of calcium ions was measured, which is the reason for their weak attachment (Liu, Xu, & Masliyah, 2004).

2.4.2. Illite

The isomorphic substitution of illite mainly happens in the tetrahedron sheet in which Si is replaced by Al and the charge is compensated by ions located in the hexagonal holes. As a result, illite unit layers are bound strongly by compensating ions and cation exchange capacity is low. The cation exchange of illite mainly occurs at the edges.

Slime coating of bitumen by illite was found in the presence of Mg^{2+} at pH 8.5 in ideal system but no slime coating was found in the alkaline tailing water (Ding et al., 2008). However, slime coating was observed in the acidic environment for bitumen and illite. By force measurement, it was found that the adhesion force between illite surfaces was strong, and the repulsive force was weak due to divalent cations and low solution pH (Long, Xu, & Masliyah, 2006).

2.4.3. Montmorillonite

Montmorillonite is a three-layer clay in which one octahedron sheet is sandwiched by two layers of tetrahedron sheet (TOT). It is expandable and has high cation exchange capacity (CEC). The reason for this is that isomorphic substitution of montmorillonite happens in both tetrahedron sheet and octahedron sheet. The latter results in the permanent charge delocalized and the compensating ions located at the basal plane of the tetrahedron sheet. The interlayer binding is thus weakened due to the presence of compensating ions. Moreover, such compensating ions sitting between montmorillonite unit layers results in swelling properties. However, it should be clarified that such swelling property is not directly related to slime coating caused by montmorillonite.

Montmorillonite is believed to cause the most problems in bitumen extraction although its content is small, and it causes strong slime coating of bitumen in the presence of divalent cations (Liu et al., 2002). Bitumen recovery was reduced when montmorillonite and Ca^{2+} were co-added

(Kasongo et al., 2000). Stronger adhesion force between bitumen and montmorillonite was measured in the presence of Ca^{2+}, which was the reason for low bitumen recovery (Liu, Xu, & Masliyah, 2004b).

2.5. Slime Coating

Slime coating in bitumen extraction is referred as the attachment of fine solids to bitumen droplets. It is very detrimental to bitumen extraction, decreasing either bitumen recovery or froth quality or both. Two possible mechanisms have been proposed regarding slime coating of bitumen and clays (Masliyah, Czarnecki, & Xu, 2011). On one hand, Ca^{2+} would adsorb on the clay surface and act as a bridge to link bitumen and clay. Adsorbed clay is hydrophilic and would prevent air bubble attachment to bitumen due to its hydrophilic nature. In this case, bitumen recovery decreases. On the other hand, the adsorption of Ca^{2+} onto the clay surface would induce further adsorption of surfactants, rendering clay hydrophobic. Hydrophobized clay would attach to bitumen surface because of hydrophobic interaction. Air bubbles could still attach to hydrophobic clay-contaminated bitumen and bitumen recovery would not be affected in this case. However, such clay-contaminated bitumen would cause clay-stabilized bitumen emulsion in the froth and reduce froth quality, which is very detrimental to the later upgrading process.

DLVO theory, which is the sum of van der Waals and electrostatic interactions, is the underlying fundamental theory describing colloidal particle interactions and slime coating. However, in some cases, classical DLVO theory is not accurate when other forces are involved such as hydration and hydrophobic forces. Thus, an extended DLVO theory (EDLVO), which considers van der Waals force, electrostatic force, hydration force, and hydrophobic force is chosen to better represent colloidal particle interactions (Lyklema, 2005). Besides, some precipitation due to chemical reactions are also considered as slime. Chrysotile, dolomite, and

hydroxyapatite could be precipitated at the coal surface, which have detrimental impact on the coal flotation due to their hydrophilic properties (Wang, Peng, & Vink, 2013).

Particles are positively charged if the aqueous phase pH is lower than the isoelectric point (IEP), and particles carry negative charges if the pH is higher than the IEP. Hence, pH largely affects colloidal behavior such as aggregation or dispersion (Doymuş, 2007). Two particles would attract each other if they carried opposite charges or repel each other if their charges are of the same sign.

Few experimental methods have been used to study slime coating. Slime coating of bitumen by clays was studied by zeta potential distribution measurements using zetaphoremeter (Liu et al., 2002) and force measurement using atomic force microscope (AFM) (Liu et al., 2005). Induction time measures the time required for the attachment between an air bubble and mineral surface (Forbes et al., 2014) or bitumen surface (Gu et al., 2004). It is also used to semi-quantitively study slime coating (Yu et al., 2017). If valuable minerals are contaminated by slime, the time required for bubble attachment becomes longer. The induction time was measured to be higher in the process water in the presence of fine solids and Ca^{2+} than in the de-ionized water (Gu et al., 2003). Partition experiments could be used to quantitatively determine the amount of clay in the water phase and at the oil-water interface (Yan & Masliyah, 1994). Scanning Electron Microscope coupled with energy dispersive X-ray spectroscopy (SEM-EDS) is widely used to investigate properties of solid-liquid interfaces. It was also used to observe slime coating of many systems (Edwards, Kipkie, & Agar, 1980; Oats, Ozdemir, & Nguyen, 2010). It not only provides actual structure and morphology of the mineral surface, but also provides elemental spectrum of the surface composition. Quartz Crystal Microbalance with Dissipation (QCM-D) was used to study slime coating of bitumen by kaolinite, montmorillonite, and illite (Tamiz Bakhtiari et al., 2015).

This very sensitive technique is based on monitoring frequency and dissipation change of sensor. In addition, quantifying the clay deposited on bitumen surface could be accomplished by QCM-D.

2.6. Primary Process Aid Sodium Hydroxide

Sodium hydroxide (NaOH) is used as the primary processing aid in the oil sands industry. The addition of NaOH improves bitumen recovery. It plays many roles in the whole bitumen extraction process.

When kaolinite contacts with the aqueous solution, the departure of the compensating cations results in surface charges on the basal plane. Normally, aluminum hydroxyl surface is hydrophilic while siloxane surface is hydrophobic (Gee, Healy, & White, 1990). Increasing the solution pH to a very high value could hydrolyze the siloxane bonds to silanol groups, resulting in siloxane surface becoming hydrophilic. Thus, adding NaOH is beneficial for bitumen liberation. The degree of bitumen liberation was increased by increasing the solution pH from 7.8 to 11 (Xiang, Liu, & Long, 2018). The surface charges on the aluminum hydroxyl surface (-AlOH) are also dependent on the solution pH. Protonation happens at low pH and deprotonation happens at high pH. As a result, octahedron basal plane carries negative charge after addition of NaOH, which would be beneficial for bitumen liberation and slime coating mitigation.

When bitumen contacts water, the surfactants orient at the bitumen-water interface with hydrophilic head facing the water phase and hydrophobic tail staying in bitumen. The hydrophilic head could be protonated or deprotonated based on the solution pH. At high pH, deprotonation reaction happens, and bitumen carries negative surface charge. Moreover, increasing the pH would decrease the bitumen-water interfacial tension and is beneficial for bitumen liberation. However, negatively charged bitumen and reduced bitumen-water interfacial tension are not helpful to bitumen aeration.

2.7. Secondary Process Aid Sodium Citrate

Sodium citrate is non-toxic, environmental-friendly, and degradable. It has good affinity with Ca2+ because of the chelating effect. Xiang et al. (2019) has shown that with the addition of sodium citrate, bitumen liberation is improved and adhesion force between bitumen and silica is reduced. With the combination of sodium hydroxide and sodium citrate, the degree of bitumen liberation was shown to be highest, and the adhesion force was negligible (Xiang et al., 2019). It was found that sodium citrate promotes faster displacement of bitumen from quartz surface and reduced the final contact angle of bitumen on quartz surface during the bitumen receding process (Xiang et al., 2020). Zhang (2020) has shown that sodium citrate could effectively prevent slime coating of montmorillonite and bitumen in the ideal system. However, Zhang (2020) concluded that if slime coating caused by montmorillonite had already happen, sodium citrate was not able to remove it. Citrate acid was found to reduce the coagulation of kaolinite and solvent-diluted bitumen due to the adsorption of citrate anions on the kaolinite surface (Gan & Liu, 2008).

Chapter 3 Role of Sodium Citrate on the Interaction of Clays and Bitumen in Process Water

3.1. Introduction

Traditionally, experimental methods such as bitumen flotation or slurry rheology could be used to study slime coating (Yu et al., 2017). However, these methods are indirect and are not able to provide accurate account of slime coating phenomenon (Arnold and Aplan, 1986a). Herein, the interaction between bitumen and three kinds of clays in the process water from Aurora Plant were investigated by zeta potential distributions, QCM-D, and SEM-EDS techniques. It is highlighted that the addition of sodium citrate plays an important role on the formation of these hetero coagulations.

Zeta potential distribution measurements have been shown to be a powerful tool to study slime coating (Liu, Zhou, Xu, & Masliyah, 2002), i.e., the interaction between bitumen and fine clay particles. In a binary system, if the species carry different surface charges and do not interact with each other, they would exhibit different mobility under an applied electric field, resulting in two distinct zeta potential distributions. On the other hand, if the two species coagulate with each other, their zeta potential distribution would be a single peak. Deducing from the study of bitumen-clay interaction, the observation of two separated distribution peaks means no occurrence of slime coating, whereas the presence of one single peak means that bitumen was coated by clays.

Quartz crystal microbalance with dissipation (QCM-D) is another useful tool to study solid-liquid interaction by monitoring frequency and dissipation change. In the current study, if clay could adsorb onto bitumen-coated sensor, the measured frequency would decrease while dissipation would increase. Besides, QCM-D could also show the effect of sodium citrate by comparing frequency change with or without pumping sodium citrate solution.

SEM-EDS is a straightforward way to observe slime coating where surface morphology of clay minerals could be observed by SEM, and the composition of clay could be analyzed by EDS. Since many unknown components could interact with bitumen and cause changes in both frequency and dissipation, the bitumen-coated sensor was taken out after QCM-D experiments and studied by SEM-EDS to make sure that frequency changes were indeed caused by the interaction of clay and bitumen.

3.2. Materials and Methods

3.2.1. Materials

Three different kinds of clays, including montmorillonite, kaolinite, and illite, were purchased from Ward's Science. Process water from Aurora Plant of Syncrude Canada Ltd. was used in the current experiments for the interaction between clays and bitumen. The process water was filtered by a syringe filter (Millex Syringe Filter Unit, 0.22 μm) before use in order to remove the natural fine particles. Sodium citrate dihydrate (> 99%, Aldrich), the secondary process aid studied in all experiments, was used as received without further purification. Bitumen sample was collected from the predominantly fed to the vacuum distillation unit and was also obtained from Syncrude Canada Ltd. Milli-Q water (18.2 MΩ·cm) was prepared by Milli-Q purification system. All experiments were performed at room temperature (23 ± 1 °C) unless otherwise specified.

3.2.2. Zeta Potential Measurement

3.2.2.1. Principles of Zetaphoremeter

Zetaphoremeter IV (CAD Instrumentation), which consists of a rectangular quartz cell, laser illuminator, CCD camera, microscope, and built-in analyzing software, was used to measure the zeta potential distributions and the mean zeta potential of the clay particles, bitumen, and their mixtures in the filtered process water with or without sodium citrate.

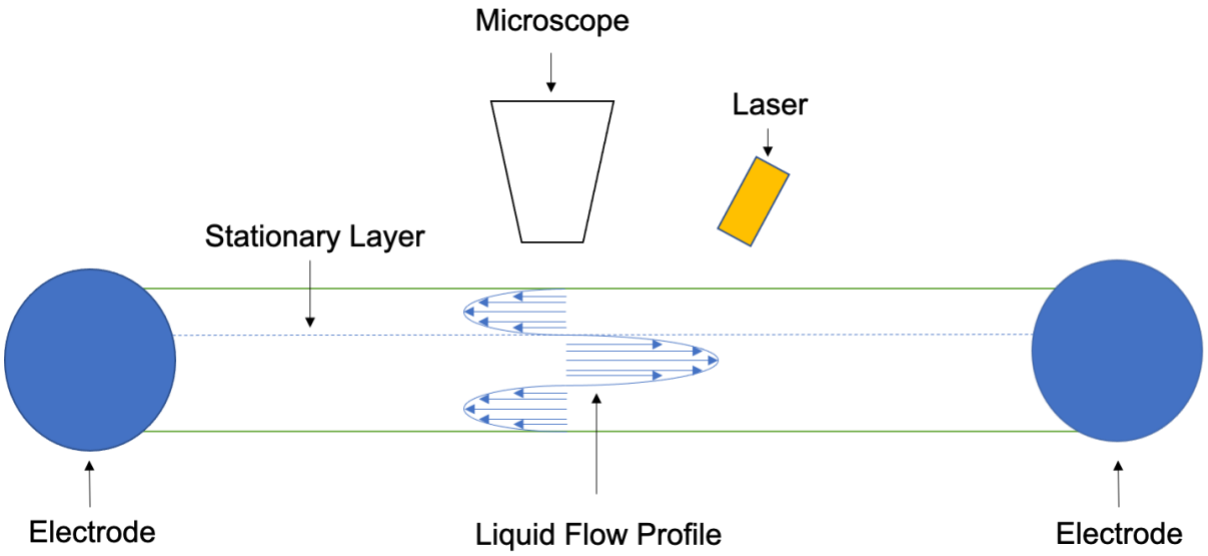

Figure 3.1. Working principle of Zetaphoremeter.

The uniform electric field is generated when the voltage is applied between electrodes at two ends of the quartz cell. Under the electric field, charged particles move from one electrode end to the other. Normally, this is also known as electrophoresis. However, the generated electric field could also drive fluid to move relative to the quartz cell due to the electrical double layer build-up at the cell-liquid interface, which is referred to as electroosmosis. During the measurement, the two ends of the quartz cell are closed and the net flow rate inside the quartz cell is zero. Thus, there must be a returning flow in the central area of the quartz cell, which is opposite to the flow near quartz cell-liquid interface. As a result, there must be two layers where the net flow rate is zero and the liquid is stationary as shown in Figure 3.1. A microscope coupled with CCD camera was focused on one of the stationary layers in order to track the movement of laser-illuminated particles. The sign and magnitude of the zeta potential were computed using the mobility of 20–50 particles. Due to the limitation of visual observation techniques, particle concentration has to be diluted in zetaphoremeter experiments. Otherwise, too many particles cause multiple scattering between illuminated particles and microscope, resulting in no trajectory of particles. Thus, 20 µl of the

original mixture solution (bitumen emulsion, clay suspension, or their mixture) was diluted by 50 ml desired solution, which had the same water chemistry as the aqueous phase of their corresponding emulsion/suspension/their mixture.

3.2.2.2. Procedure of Zeta Potential Measurements

Bitumen-in-water emulsion was first prepared by mixing 0.3 g bitumen with 30 ml filtered process water. The mixture was emulsified by a dismembrator with 70% amplitude for 30 min. Meanwhile, clay suspensions were also prepared by dispersing 0.3 g of the clay in 30 ml filtered process water and sonicating for 15 min. Finally, the bitumen-clay mixture in the process water was obtained by mixing the same volume of the as-prepared bitumen emulsion and clay suspension for another 20 min, which resulted in a 1:1 bitumen-to-clay mass ratio. To investigate the effect of sodium citrate on the hetero-coagulation of bitumen and clay, 1 mM of Na_3Cit was added in both bitumen emulsion and clay suspension before they were mixed together. Afterward, the mixture of bitumen and clay was prepared by mixing and sonicating the bitumen emulsion and clay suspension, where 1 mM Na_3Cit had already been added. During the measurement, samples were first pulled into the quartz cell by a syringe. The movements of particles under the electric field were recorded by the camera equipped on the Zetaphoremeter. The values of the zeta potential could be obtained by the mobility of particles using the Smoluchowski equation:

$$u_e = \frac{\varepsilon\zeta}{\eta} \tag{3.1}$$

where ε is permittivity, η is viscosity, u_e is mobility, and ζ is zeta potential. Histogram of mobilities and zeta potential were then given by the software. Each condition was repeated three times. Due to the limitation of Zetaphoremeter technique in the current research for anisotropic clays, the result obtained is the average value of the zeta potential of clay rather than that of different faces of clay.

3.2.3. Measurements of Clay Adsorption on Bitumen by Quartz Crystal Microbalance with Dissipation

3.2.3.1. Working Principles of QCM-D

QCM-D sensor is a piece of quartz crystal with conducting metal on each side. Because of the piezoelectric property of quartz crystal, QCM-D sensor oscillates at a certain resonance frequency under the alternating electric voltage. The resulting frequency is dependent on the mass of the materials deposited on the sensor (Chen, Xu, Liu, Masliyah, & Xu, 2016). Thus, the mass can be related to the frequency, which is calculated by the Sauerbery relationship Eq. 3.2.

$$-\Delta f = \frac{n f_0 \Delta m}{\rho_q t_q} = \frac{n \Delta m}{C} \tag{3.2}$$

where n is the harmonic number, f_0 is the fundamental resonance frequency, ρ_q is the density of quartz, t_q is the thickness of quartz crystal, and C is the sensitivity constant (17 ng·cm^{-2}·Hz^{-1} for 5 MHz sensor).

During the oscillation, an ideal solid exhibits a complete elastic property and energy is stored completely. However, not all of the deposited materials are rigid. Soft materials have viscoelasticity, so that the energy is dissipated when the sensor oscillates. Therefore, the Sauerbrey relationship is not capable of describing such systems. In this situation, it is better to consider dissipation and define the loss energy divided by the stored energy as dissipation (Xiang, Liu, & Long, 2018). Given by eq 3.3, the dissipation is calculated as

$$D = \frac{E_D}{2\pi E_S} \tag{3.3}$$

where E_D is the energy, and E_S is the energy stored during the oscillation.

3.2.3.2. Preparation of Bitumen-Coated QCM-D Sensor.

SiO_2 (QSX 999, Q-Sense) sensors were first treated by UV/Ozone for 10 mins and rinsed by acetone. The sensors were then rinsed by Milli-Q water and blew by nitrogen gas to ensure a clean surface. After that, the cleaned sensors were dipped in the 0.1 vol% octadecylchlororsilane/toluene for 30 s to make the sensor surface hydrophobic. Such sensors were then rinsed by toluene and acetone, followed by blowing with nitrogen gas. The contact angle of the hydrophobized sensor was measured to be ~70°.

A layer of bitumen was coated on the hydrophobized SiO_2 sensor through spin coating. Prior to depositing bitumen on the hydrophobic sensor, toluene-diluted bitumen (5 wt.%) was centrifuged and filtered to remove possible fine solids. During the spin coating process, a hydrophobized SiO_2 sensor was rotating on a spin coater (Laurell WS-400A-6NPP/Lite) at 2500 rpm for 40 s, while 5 drops of the diluted bitumen were carefully dripped onto the sensor at an approximate speed of one drop every 10 s. After the deposition of diluted bitumen solution, an additional 40 s rotation at 5000 rpm was conducted to remove residual toluene solvent. Before the QCM-D experiments, bitumen-coated sensors were left overnight to evaporate the remaining toluene.

3.2.3.3. Procedure of QCM-D Measurements

QCM-D was used to measure the adsorption of clay particles onto the bitumen-water interface under process water environment with or without the presence of sodium citrate. To eliminate the deposition of the clay onto bitumen-coated sensor due to sedimentation, the QCM-D chamber was put reversely, so that the frequency change is the only result of the interfacial adsorption of clay onto bitumen. The flow rate of all experiments was kept at 0.1 ml/min. In each experiment, Milli-Q water was pumped to flow over bitumen-coated sensor as the baseline. The pumping liquid was

switched from Milli-Q water to process water as the second baseline to look at the frequency and dissipation change due to the adsorption of components in the process water onto bitumen. In the next step, the fluid was switched to process water containing clay with the concentration of 0.001 g/ml. Afterwards, the fluid was switched back to process water to remove any possible loosely bounded clay. In the experimental investigation of the effect of sodium citrate, the procedure and the sequency of introducing liquid were repeated in the same order as mentioned above, except that 1 mM Na_3Cit was added in the process water.

3.2.4. Scanning Electron Microscopy – Energy dispersive X-Ray Spectroscopy (SEM/EDS)

In this work, the bitumen-coated sensors were collected after QCM-D experiments and analyzed by SEM, which could visually demonstrate the montmorillonite adsorption on the bitumen surface. Moreover, combining with energy dispersive X-ray spectroscopy (EDS), the element composition of the adsorptions could be identified, which could provide further evidence on the slime coating.

3.3. Results and Discussion

3.3.1. Zeta Potential Distributions of Individual Clays and Bitumen

Zeta potential of bitumen and three kinds of clays (montmorillonite, kaolinite, and illite) were measured individually in process water. After that, the water chemistry was changed to 1 mM Na_3Cit in process water, and zeta potentials of these colloidal systems were measured again to study the effect of sodium citrate.

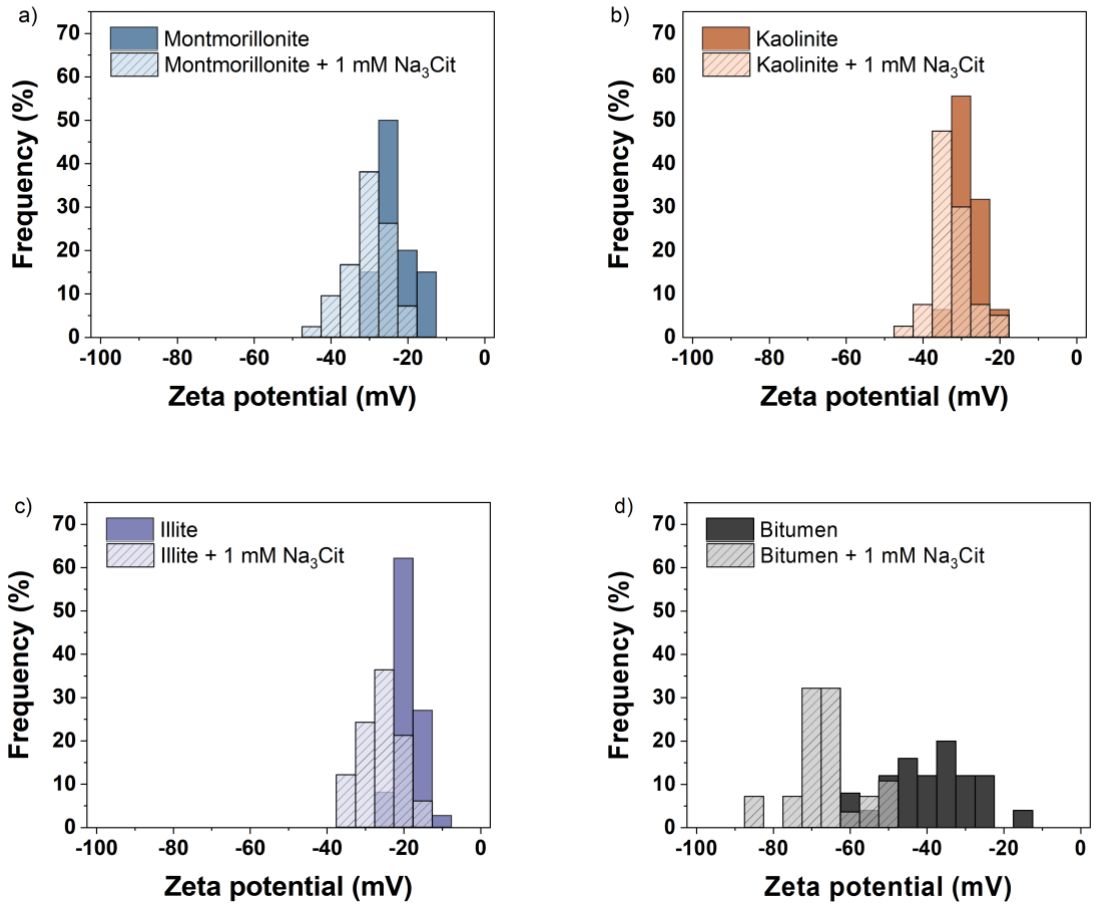

Figure 3.2. Effect of 1 mM Na_3Cit on the zeta potential distributions of a) montmorillonite and b) kaolinite c) illite and d) bitumen in the process water.

Figure 3.2a shows the zeta potential distributions of montmorillonite in process water with or without 1 mM sodium citrate. In the absence of sodium citrate, the mean zeta potential of montmorillonite was centered at -25.8 mV, and it decreased to -32.3 mV if 1 mM Na_3Cit was introduced to the process water. For non-swelling clays, the addition of 1 mM Na_3Cit changed the zeta potential of kaolinite from -30.8 mV to -35.2 mV (Figure 3.2b), while the zeta potential of illite also became more negative from -21.5 mV to -28.0 mV after Na_3Cit addition (Figure 3.2c). The effect of Na_3Cit on bitumen in process water is shown in Figure 3.2d. It indicated that bitumen

surface also became more negatively charged in the presence of Na_3Cit. In the process water, the mean zeta potential of bitumen was measured to be -41.3 mV, which was very close to the results in the literature (Zhao et al., 2006). With the addition of 1 mM Na_3Cit, the zeta potential of bitumen became more negative (-68.8 mV). From Figure 3.2, it could be concluded that the addition of Na_3Cit would make the zeta potential of both clay and bitumen surfaces more negatively charged.

3.3.2. Zeta Potential Distributions of Bitumen-Clay Mixtures

Zeta potential of bitumen-montmorillonite mixture in process water is shown in Figure 3.3a. A single peak located between the mean zeta potential of bitumen and montmorillonite was observed, which was the result of slime coating between bitumen and montmorillonite in the process water. The single peak was very close to the mean zeta potential of montmorillonite, indicating a strong attachment of montmorillonite particles onto bitumen droplets.

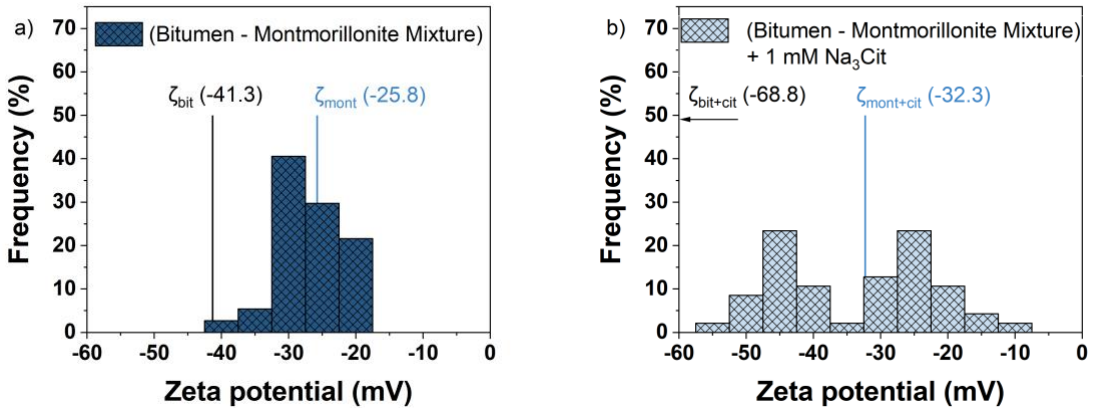

Figure 3.3. Zeta potential distributions of bitumen-montmorillonite mixture in the process water: a) without Na_3Cit, and b) with 1 mM Na_3Cit.

The presence of Na_3Cit could prevent slime coating if it was added before the mixing of bitumen emulsion and montmorillonite suspension. As presented in Figure 3.3b, the mixture showed two distinct peaks. Such a result indicates the possible effect of Na_3Cit on preventing the

hetero-coagulation of bitumen and montmorillonite. However, it should be noted that the values of two peaks were different from bitumen and montmorillonite measured independently before, and these values shifted closer to each other. This phenomenon could be explained by the hydrodynamic interactions between the moving bitumen and montmorillonite at the various electrophoretic mobilities, which is also known as electrokinetic retardation (Hunter, 1981).

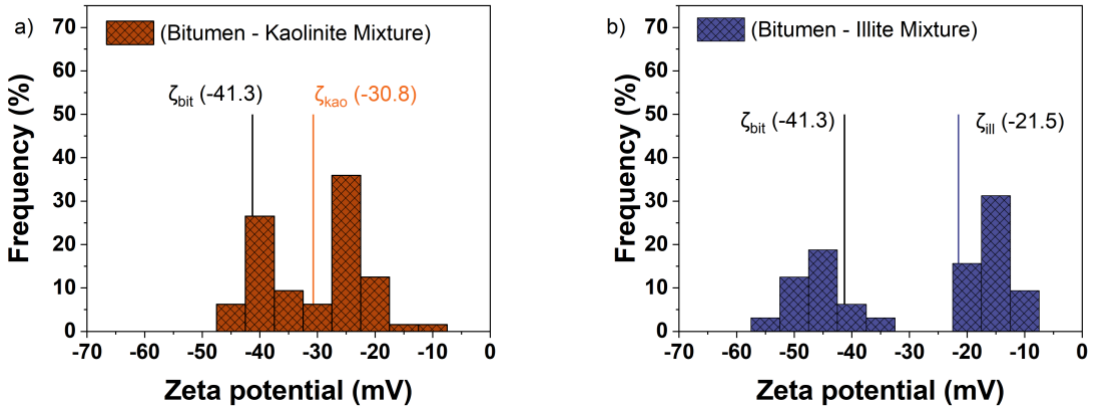

Figure 3.4. Zeta potential distributions of a) mixture of bitumen and kaolinite and b) mixture of bitumen and illite in the process water.

Both kaolinite and illite did not interact with bitumen in the process water. The mixture of kaolinite and bitumen was prepared using the same protocol described above. As shown in Figure 3.4a, the zeta potential of the mixture of kaolinite and bitumen in the process water showed two separated distributions, suggesting no slime coating of bitumen by kaolinite. Two distinct distributions of zeta potential of the mixture of illite and bitumen are shown in Figure 3.4b, which again indicated no hetero-coagulation between bitumen and illite.

3.3.3. Adsorption of Clays on Bitumen

QCM-D technique was used to further study the effect of sodium citrate on interactions of bitumen and clay particles in the process water. According to the results obtained from

Zetaphoremeter, it is reasonable to hypothesize that montmorillonite particles should exhibit strong adsorption onto bitumen surface, whereas that of kaolinite and illite is suspectable.

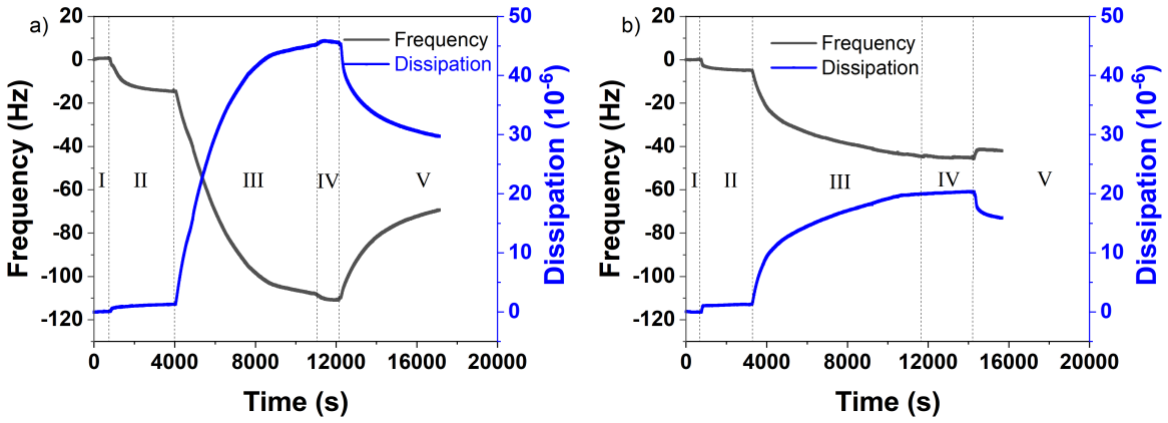

Figure 3.5. Change in frequency and dissipation of bitumen coated sensor a) without Na_3Cit and b) with 1 mM Na_3Cit. Dash lines in a) indicate fluid was pumped in the sequence of Milli-Q water, process water, process water containing montmorillonite, process water, and Milli-Q water. Dashed lines in b) indicate fluid was pumped in the sequence of Milli-Q water, process water with added 1 mM Na_3Cit, process water with added 1 mM Na_3Cit containing montmorillonite, process water with 1 mM Na_3Cit, and Milli-Q water.

QCM-D results are illustrated in Figure 3.5. During QCM-D experiments, Milli-Q water was first pumped in the first 600 s (step I), and then the filtered process water was injected for ~2000 s (step II). It can be seen from Figure 3.5a that the frequency decreased to 14 Hz and the dissipation increased slightly. After both frequency and dissipation remained unchanged in step II, the process water containing montmorillonite was introduced. The frequency showed a significant negative shift to about -115 Hz and the dissipation showed a positive shift to 45. Such sharp changes in frequency and dissipation in step III suggested strong adsorption of montmorillonite onto bitumen surface in the process water. Since the flow cell was put reversely, the adsorption was the only

result of the interaction of montmorillonite and bitumen, and the impact of gravitational sedimentation was negligible. Later, the fluid was switched to particle-free process water to wash off the particles which were loosely adsorbed at the bitumen surface. However, there were no decrease on neither frequency nor dissipation in step IV, indicating that the slime coating caused by bitumen-montmorillonite interaction is irreversible in the process water environment.

The effect of Na_3Cit on the adsorption of montmorillonite by bitumen is shown in Figure 3.5b. Step I was the same as before where Milli-Q water was pumped into the chamber to establish a baseline. In step II, process water containing 1 mM Na_3Cit was pumped into the flow cell. The changes of frequency and dissipation became less significant with the presence of Na_3Cit, suggesting less component in process water was adsorbed onto bitumen. Such a phenomenon is most likely due to the chelation of divalent cations by Na_3Cit. Later, the fluid was switched to montmorillonite in the process water containing 1 mM Na_3Cit (step III). It was noted that the frequency decreased to ~ 40 Hz and the dissipation increased to ~ 20 when they reached steady state. Compared with the same step III in Figure 3.5a, much less changes were found in both frequency and dissipation, demonstrating the inhibiting effect of Na_3Cit on the formation of bitumen-montmorillonite hetero-coagulation. Although 1 mM Na_3Cit was added in the process water, there were still some changes in frequency and dissipation, indicating that the prevention of slime coating was not complete. This is likely because 1 mM Na_3Cit was not enough to consume all the divalent cations in the process water. Besides, the very high ionic strength in the process water compressed the electric double layer, resulting in the attractive VDW force to dominate over the repulsive EDL force in the long range.

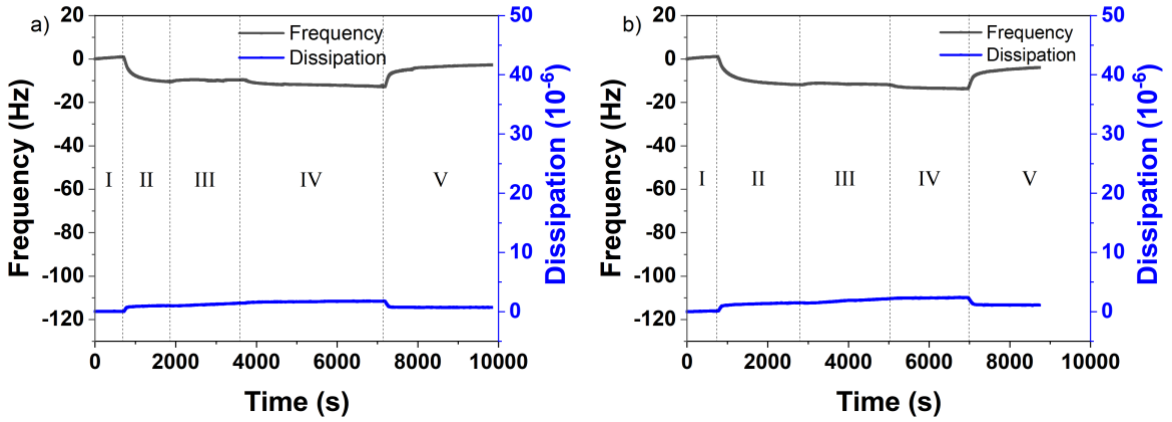

Figure 3.6. Change in frequency and dissipation of bitumen coated sensor where a) kaolinite and b) illite were introduced. Dashed lines in a) indicate fluid was pumped in the sequence of Milli-Q water, process water, process water containing kaolinite, process water, and Milli-Q water. Dashed lines in b) indicate fluid was pumped in the sequence of Milli-Q water, process water, process water containing illite, process water, and Milli-Q water.

Previous experiments regarding zeta potential measurements indicated no slime coating of bitumen by kaolinite nor illite. In order to verify the conclusions obtained from zeta potential measurements, QCM-D was used to further verify that there is no adsorption of kaolinite or illite onto the bitumen-water interface. Experiments were conducted following the previous OCM-D experimental steps, where fluids were pumped into the QCM-D chamber by the same order.

As shown in Figure 3.6a, the Milli-Q water was pumped for ~600 s to establish a baseline in step I, the filtered process water was then pumped for ~2000 s as shown in step II to see if there is possible adsorption of some components onto bitumen. It could be seen from step II of Figure 3.6a that the frequency decreased to 14 Hz and the dissipation increased a little, which was the possible adsorption of the components in the process water onto the bitumen-water interface. After both changes of frequency and dissipation reached equilibrium, the process water containing kaolinite

was introduced in step III. No significant changes in frequency and dissipation were observed, indicating no adsorption of kaolinite onto bitumen. Later, the fluids were pumped in the order of process water and Milli-Q as shown in steps IV and V. In step IV, both changes in frequency and dissipation could be negligible, whereas the frequency increased, and the dissipation decreased in region V, indicating that some components were washed off by Milli-Q water.

The fluids were the same as previous experiments for montmorillonite and kaolinite except that in step III, process water containing illite was pumped into the QCM-D chamber. Similar results could be obtained for illite in region III in Figure 3.6b, in which there was no noticeable adsorption of illite onto the bitumen-water interface.

3.3.4. Studying Slime Coating by SEM/EDS

After QCM-D experiments, sensors were taken out and analyzed using Scanning Electron Microscopy coupled with Energy Dispersive X-ray spectroscopy to verify the slime coating of montmorillonite on the bitumen surface.

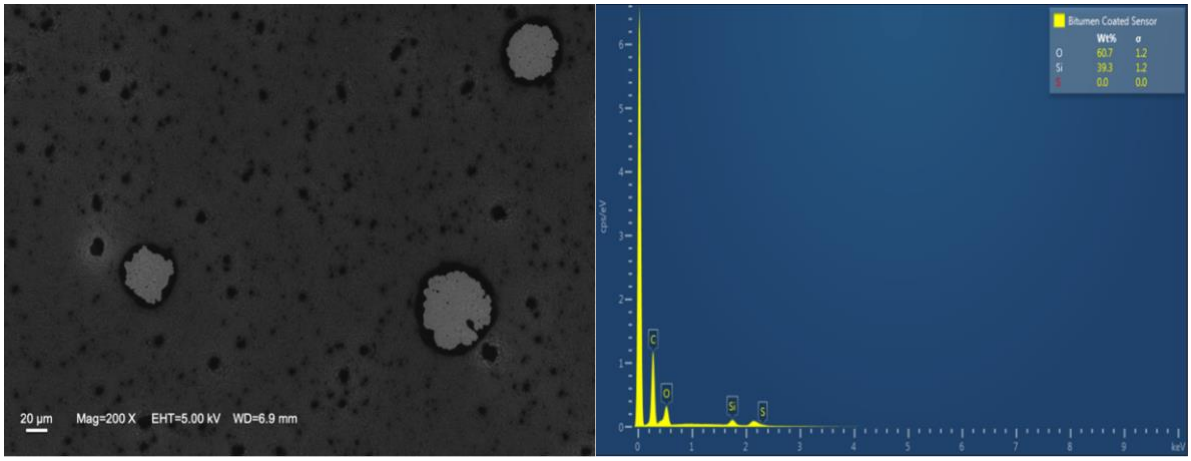

Figure 3.7. SEM image and EDS analysis of bitumen coated sensor.

SEM and EDS maps shown in Figure 3.7 were the original bitumen coated sensor without slime coating. EDS analysis of Figure 3.7 showed high contents of C and O peaks, which should be attributed to the hydrocarbon components in bitumen. Black parts of SEM image in Figure 3.6 also indicated C-group in bitumen.

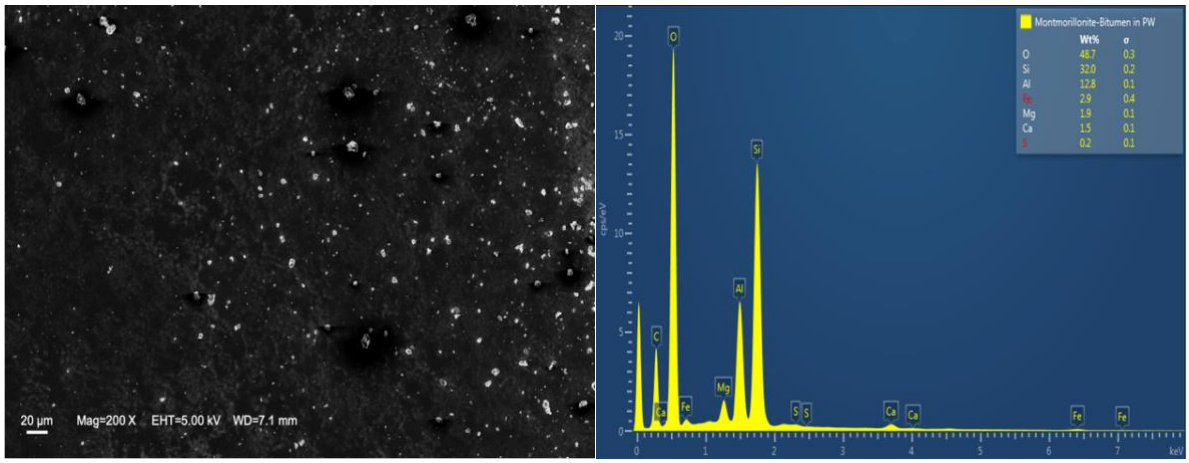

Figure 3.8. SEM image and EDS analysis of montmorillonite contaminated bitumen coated sensor.

As shown in Figure 3.8, SEM image clearly showed many white dots on the bitumen sensor, and EDS analysis of chemical peaks confirmed that the main components of white dots were clays. In the EDS analysis showen in Figure 3.8, the scanned samples were mainly composed of Al and Si, which are the characteristic elements of montmorillonite. Besides, there were Fe peaks in the EDS spectrum, indicating some isomorphic substitutions of Al by Fe.

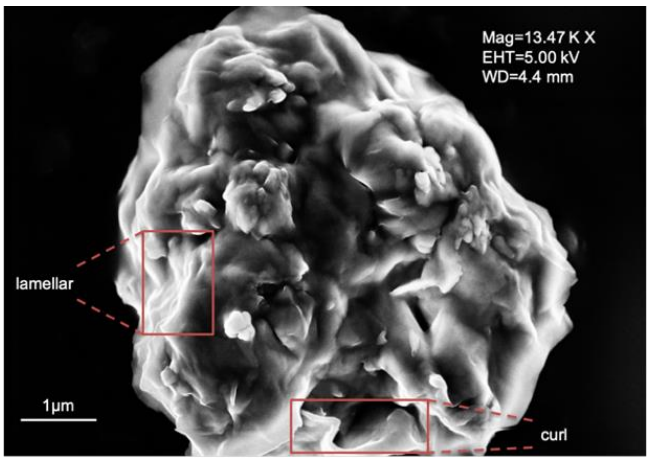

Figure 3.9. Morphology of montmorillonite particle engulfed in bitumen.

Details of single particle in Figure 3.9 showed the morphology and structure of clay. Both the lamellar and curl structure are very unique features of clay. Therefore, Figures 3.8 and 3.9 explicitly suggest that bitumen was slime-coated by montmorillonite in the process water.

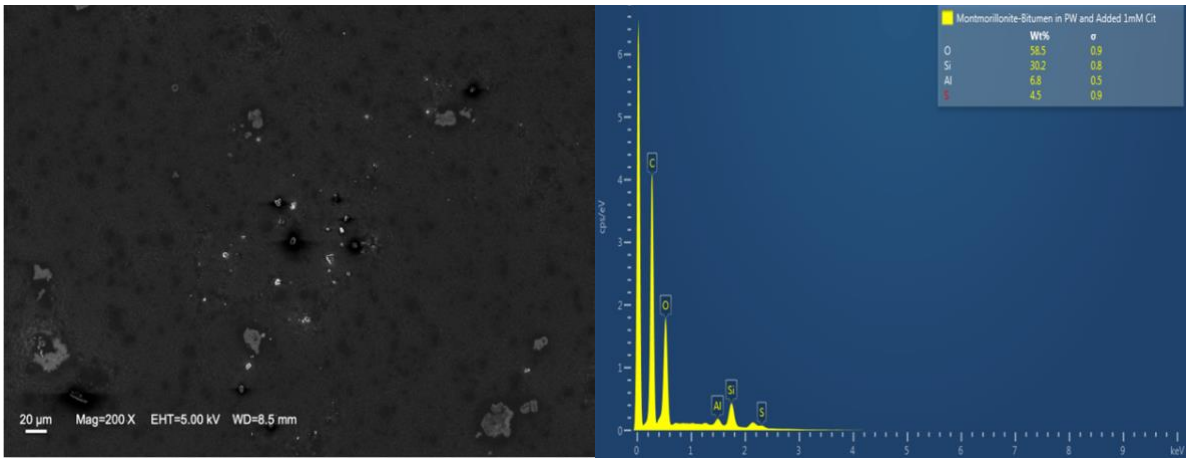

Figure 3.10. SEM image and EDS analysis of bitumen coated sensor. 1 mM Na_3Cit was added in the pumped fluids (process water and process water containing montmorillonite).

Figure 3.10 shows the SEM and EDS of the bitumen sensor, on which 1 mM Na_3Cit was added in the process water. Compared with Figure 3.8, the SEM image in Figure 3.10 showed fewer white dots, and EDS analysis of Si and Al showed much less counts, indicating a reduced slime coating when Na_3Cit was introduced.

3.4. Conclusions

Three experimental techniques have been used to study the slime coating of bitumen by clays and the effect of sodium citrate on slime coating. In the process water from the Aurora Plant, montmorillonite was shown to strongly interact with bitumen and cause severe slime coating. Such a slime coating phenomenon could be prevented by adding sodium citrate. On the other hand, no slime coating was found between bitumen and non-swelling clay (e.g., kaolinite and illite) based on current results.

Chapter 4 Synergistic Effect of Sodium Citrate and Sodium Hydroxide on the Interaction of Real Fines and Bitumen in Process Water

4.1. Introduction

In the previous chapter, experiments mainly focused on the interaction of bitumen and clays in the process water from the Aurora Plant. However, real clays in oil sands extraction process are not always ideal. In order to reveal more insights regarding the synergistic effect of NaOH and Na_3Cit, as well as to provide a more reliable guidance to industrial operations, interaction of bitumen and real fines from oil sands were investigated. Besides, the effect of the dosage of NaOH and its combined effect with Na_3Cit on preventing slime coating were also studied.

4.2. Materials and Methods

4.2.1. Materials

Three kinds of real fines and process water from Plant 5 of Syncrude Canada Ltd. were used in the current experiments. The pH of process water under different experimental conditions is given in Table 4.1. Among the three kinds of fines, two were labeled with No. 18 and No. 23, and the third was collected by combining and mixing No. 53, No. 54, No. 55, No. 56, No. 57, and No. 58 fines as one sample. Information about the samples is given in Table 4.2. The process water was filtered by a syringe filter (Millex Syringe Filter Unit, 0.22 μm) before use in order to remove the fine particles. Sodium citrate dihydrate (> 99%, Aldrich), the secondary process aid studied in this chapter, was used as received without further purification. Bitumen sample was collected from the predominantly fed to the vacuum distillation unit and was also obtained from Syncrude Canada Ltd. Milli-Q water (18.2 MΩ · cm) was prepared by Milli-Q purification system. All experiments were performed at room temperature (23 ± 1 °C) unless otherwise specified.

Table 4.1. pH of process water with added chemicals

pH	NaOH mM	Na_3Cit mM
8.43	0	0
8.57	0	1
10.32	5	0
10.35	5	1
11.63	10	0
11.63	10	1
12.15	15	0
12.16	15	1

Table 4.2. Information of real fines extracted from oil sands

#	Cap #	Sample ID	Sample Description	Memo
1	18	E194014	NM 2017·424#14	
2	23	E194020	NM 2017·402#20	
3	53	E189179	NM 2017·412#29	Combine and mix well as one sample
	54	E189177	NM 2017·415#27	
	55	E189184	NM 2017·431#34	
	56	E189185	NM 2017·431#35	
	57	E189186	NM 2017·431#36	
	58	E189193	NM 2017·421#44	

4.2.2. Wettability Modification of Kaolinite

The surface wettability of kaolinite was modified to study the relationship between slime coating and solid wettability. Figure 4.1 shows the procedure of wettability alternation for kaolinite. Bitumen was first dissolved in toluene with the concentration of 5 wt.%. Kaolinite was then added in the toluene-diluted bitumen and stirred for 24 hours to reach maximum contact with components in bitumen. The suspended kaolinite settled down very fast due to negligible EDL repulsion in the organic phase. The solid and liquid were separated, and the supernatant was discharged. Fresh toluene was used to wash the solids for several times until the supernatant became colorless. The as-prepared hydrophobized kaolinite was dried in the oven overnight before conducting experiments.

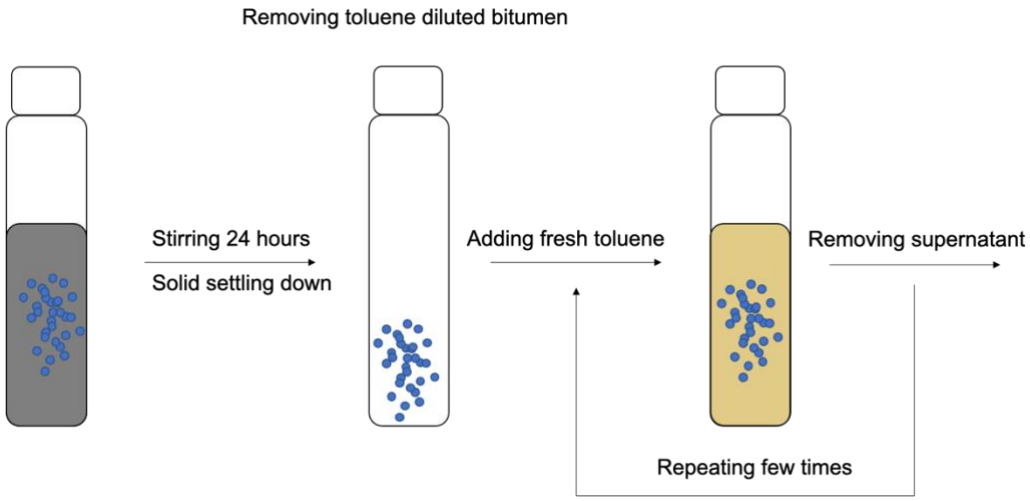

Figure 4.1. Experimental procedure of wettability modification of kaolinite.

4.3. Results and Discussion

4.3.1. Effect of Clay Wettability on Slime Coating

Previous results showed that there was no slime coating between bitumen and non-swelling clays, such as kaolinite and illite. However, such a conclusion may not be applicable to real fines

since there are many differences between clays and real fines, especially when discussing the surface hydrophobicity. Therefore, the hydrophobicity of kaolinite was altered by bitumen contamination and the effect of solid hydrophobicity on slime coating is discussed in this chapter.

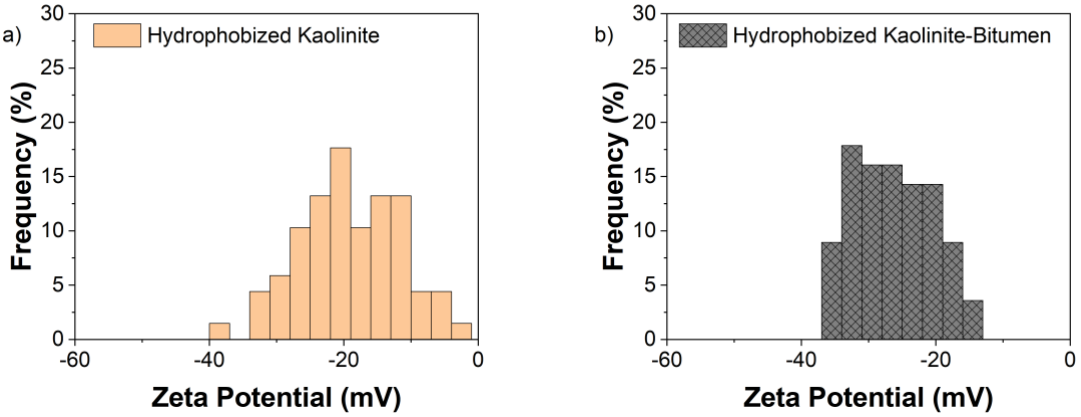

Figure 4.2. Zeta potential distributions of a) hydrophobized kaolinite and b) mixture of bitumen and hydrophobized kaolinite in the process water.

Figure 4.2a shows the zeta potential distribution of hydrophobized kaolinite, which was prepared by the above-mentioned method. As shown in Figure 4.2b, when hydrophobized kaolinite and bitumen were mixed together, only one single distribution of zeta potential was observed. Contrary to previous results where kaolinite did not interact with bitumen, current contaminated kaolinite caused slime coating. It is believed that the wettability of solids plays a role on slime coating. The possible underlying mechanism may be the hydrophobic interaction(Liu et al., 2003).

4.3.2. Synergistic Effect of NaOH and Na_3Cit on the Zeta Potential of Real Fines

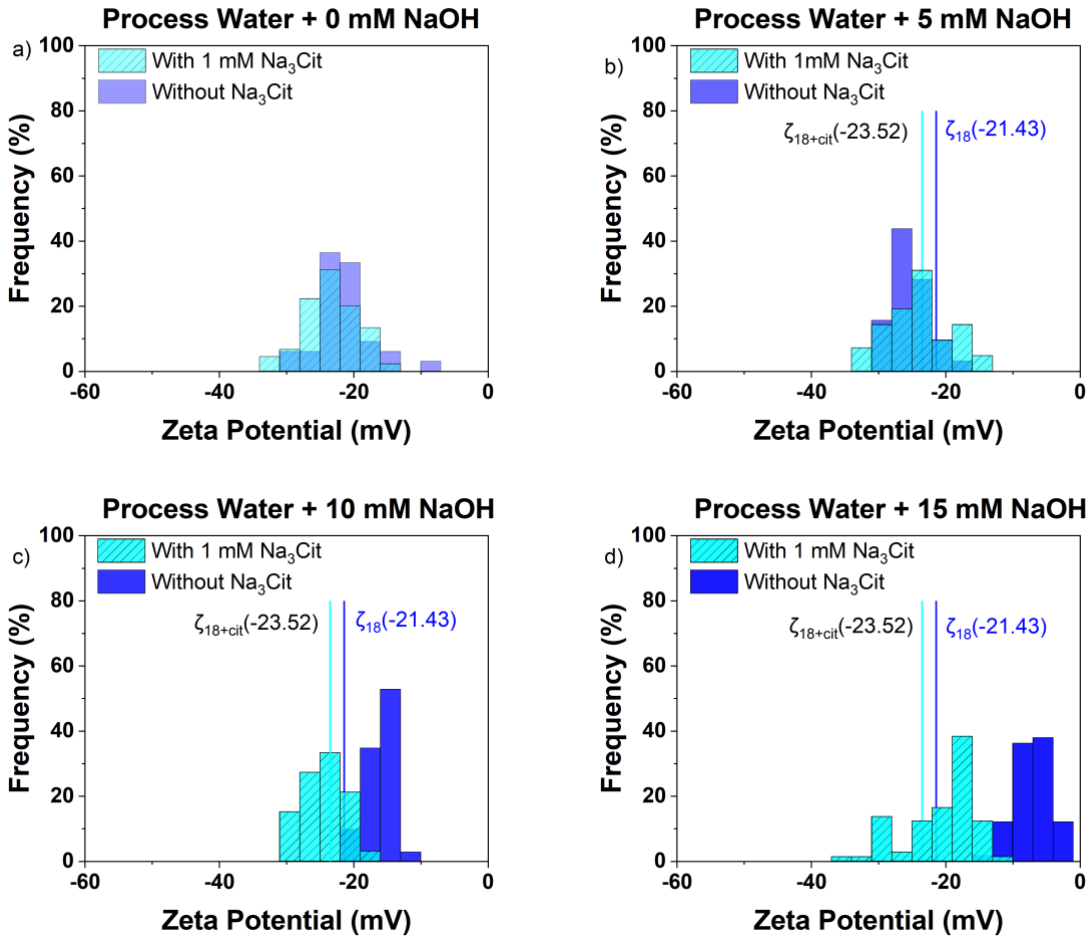

Figure 4.3. Effect of Na_3Cit and NaOH dosage on the zeta potential distribution of No. 18 fines in the process water from Plant 5. The concentration of NaOH was changed from a) 0 mM to b) 5 mM to c) 10 mM and to d) 15 mM.

The mean zeta potential of No. 18 fines in the process water shifted a little bit negative from -21.43 mV to -23.52 mV, when 1 mM Na_3Cit was added to the process water, which was not a significant change as shown in Figure 4.3a. The two zeta potential distributions of No. 18 fines were almost totally overlapping with and without Na_3Cit addition. Such a result suggests that Na_3Cit may not have an effect on changing the zeta potential of No. 18 fines in the process water

from Plant 5. As shown in Figure 4.3b, although the distributions of zeta potentials still overlapped in two cases (5 mM NaOH addition alone, and 5 mM NaOH + 1 mM Na_3Cit), they both became more negative as compared in Figure 4.3a. This suggests that NaOH and Na_3Cit influenced the zeta potential of No. 18 fines. When the dosage of NaOH was increased to 10 mM as shown in Figure 4.3c, the zeta potential of No.18 fines became less negative, which was contrary to when 5 mM NaOH was added as shown in Figure 4.3b. The contradictory results may be due to the increased ionic strength and compression of the electrical double layer. However, it should be noted that if 10 mM NaOH and 1 mM Na_3Cit were added together, although the ionic strength was even higher, the zeta potential of No. 18 fines still shifted to more negative as compared with no addition of Na_3Cit. Figure 4.3d showed more obvious results than Figure 4.3c. In the presence of 15 mM NaOH, the magnitude of the zeta potential of No. 18 fines became even smaller than adding 10 mM NaOH as shown in Figure 4.3c. However, in the presence of 15 mM NaOH, adding 1 mM Na_3Cit significantly shifted the distributions to more negative.

Overall, the effect of NaOH and Na_3Cit and their combined effect on the mean zeta potential of No. 18 fines are shown in Figures 4.3a-d. Increasing the concentration of NaOH from 0 to 15 mM shifted the zeta potential distribution to more negative due to added OH^- and increased pH, but it became less negative at a higher concentration of NaOH due to increased ionic strength. With the addition of Na_3Cit, the zeta potential distribution shifted to more negative again and such phenomenon was more obvious at high dosage of NaOH.

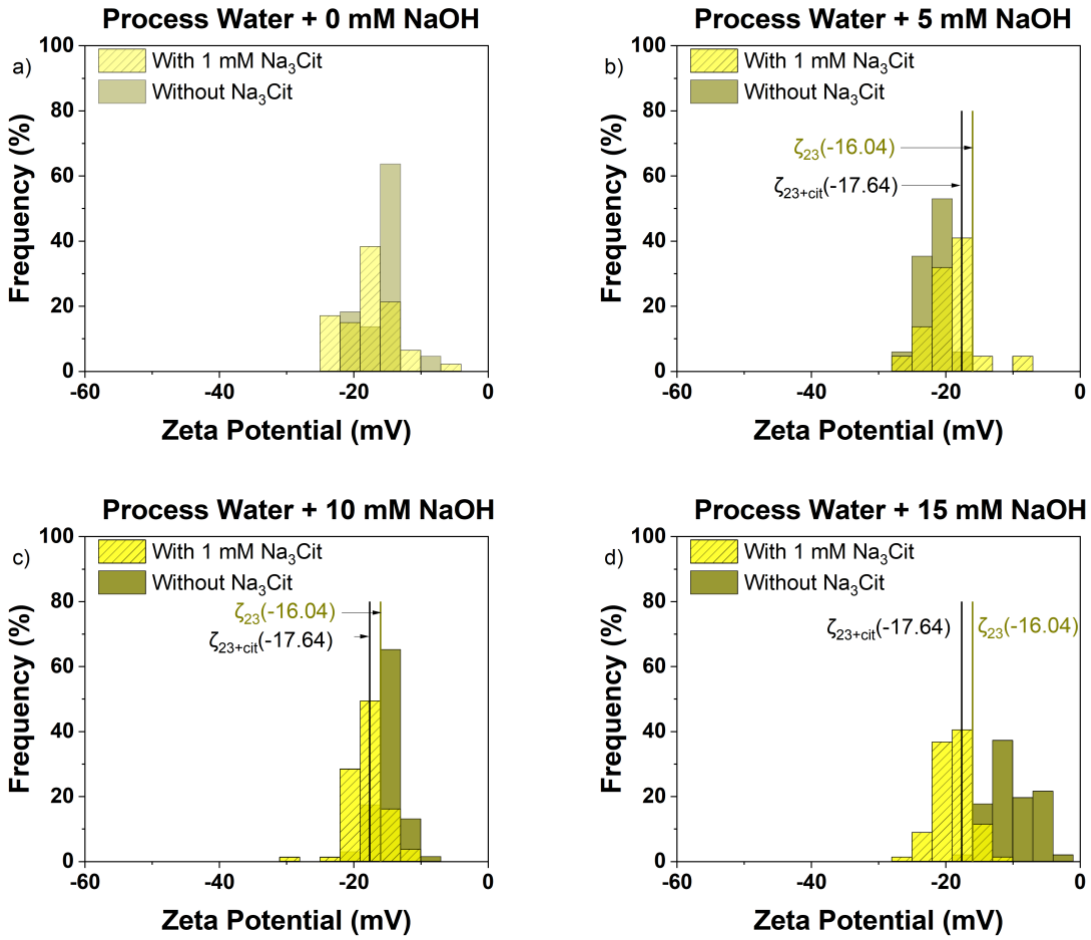

Figure 4.4. Effect of Na_3Cit and NaOH dosage on the zeta potential distribution of No. 23 fines in the process water from Plant 5. The concentration of NaOH changed from a) 0 mM to b) 5mM to c) 10 mM and to d) 15 mM.

It could be observed from Figure 4.4a that the mean zeta potential of No. 23 fines in the process water shifted from -16.04 mV to -17.64 mV after 1 mM Na_3Cit was added, indicating the negligible effect of Na_3Cit on changing the zeta potential of No. 23 fines. If 1 mM Na_3Cit and 5 mM NaOH were added together, zeta potentials shifted negatively, but still overlapped with the case of 5 mM NaOH (Figure 4.4b). When the concentration of NaOH was increased to 10 mM, it could be seen that the zeta potential of No. 23 fines after Na_3Cit was added was more negative

than that without Na_3Cit (Figure 4.4c). This finding became more obvious after increasing the concentration of NaOH to 15 mM, which is shown in Figure 4.4d. In the presence of 15 mM NaOH, two distributions where Na_3Cit was added or not became far away from each other. Besides, it should be noted that with the increasing of NaOH concentration from 0 to 15 mM, the magnitude of the zeta potential became smaller, showing the same results as above in Figure 4.3. When the dosage of NaOH was increased, at high dosage such as 15 mM, Na_3Cit was able to make the zeta potential of No. 23 fines more negative.

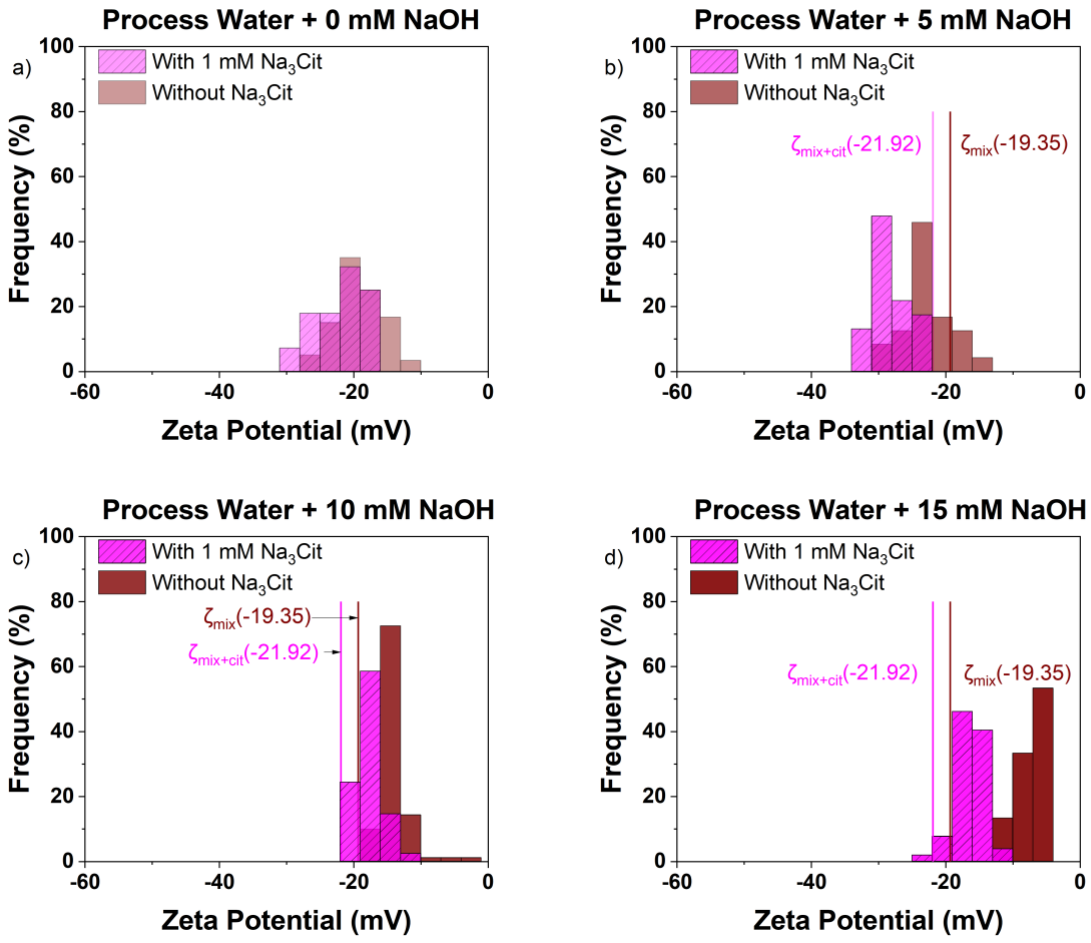

Figure 4.5. Effect of Na_3Cit and NaOH dosage on the zeta potential distribution of mixed fines in the process water from Plant 5. The concentration of NaOH changed from a) 0 mM to b) 5mM to c) 10 mM and to d) 15 mM.

No.53-No.58 fines were mixed as one sample, which was labeled as ‘mixed fines’. Effects of NaOH and Na_3Cit on the zeta potential of mixed fines have shown similar results as No. 18 and No. 23 fines. As illustrated in Figure 4.5a, the zeta potential distributions of mixed fines, in which no chemicals were added and 1 mM Na_3Cit was added, were relatively comparable. When the concentration of NaOH was increased in Figures 4.5b, c, & d, the zeta potential of mixed fines became more negative at first and then less negative. Such changes in the zeta potential of mixed fines were similar to what happened on the previous two kinds of fines. Similarly, Na_3Cit showed synergistic effect with NaOH on changing the zeta potential where in Figures 4.5b-d, added Na_3Cit shifted the zeta potential to more negative.

In conclusion, the above results in Figures 4.3 to 4.5 show that Na_3Cit alone did not change the zeta potentials of real fines, whereas NaOH could change the zeta potentials by depressing the electrical double layer. More importantly, NaOH and Na_3Cit showed synergistic effect on changing the zeta potentials.

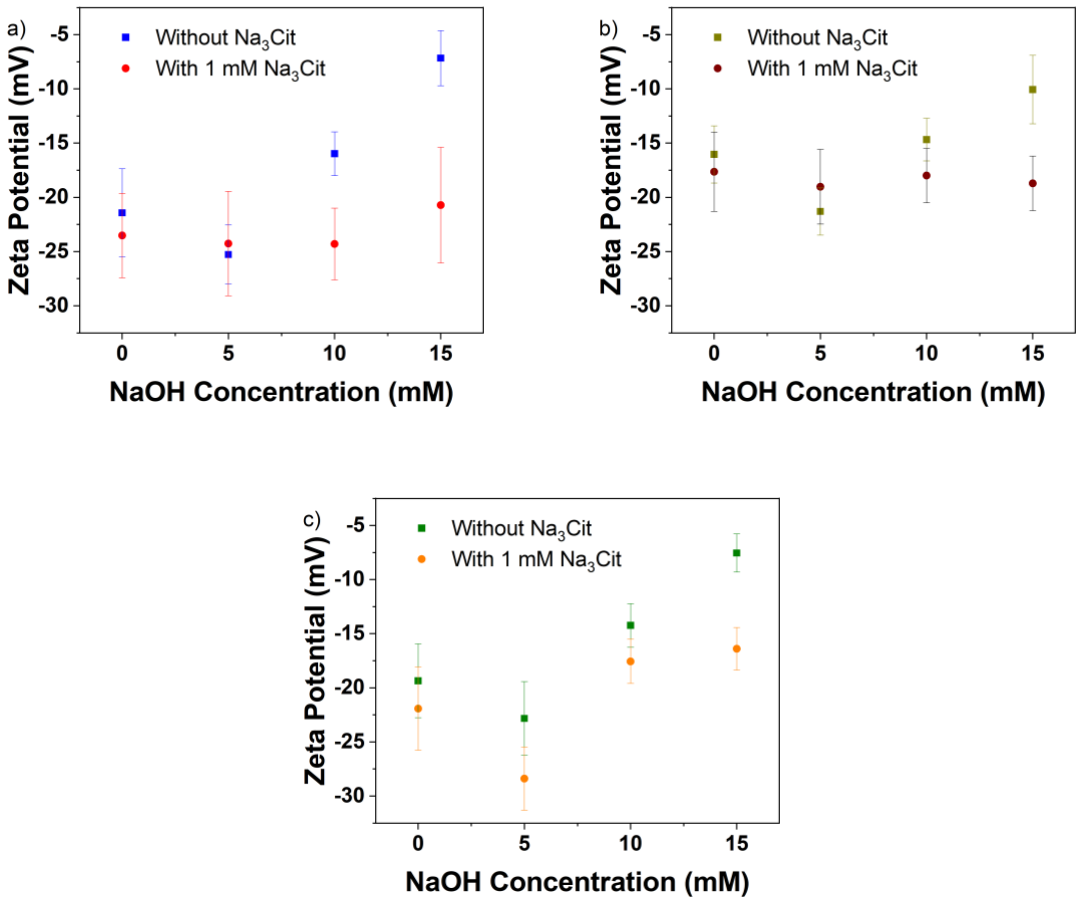

Figure 4.6. Effect of Na_3Cit and NaOH dosage on the mean zeta potential of a) No. 18 fines b) No. 23 fines and c) Mixed fines in the process water from Plant 5.

Overall, the mean zeta potential of three kinds of fines in the presence of different dosage with or without the addition of Na_3Cit are depicted in Figure 4.6. It is very clear that with the increasing dosage of NaOH, the mean zeta potential of all of three fines similarly became less negative, while even at high dosage of NaOH, 1 mM Na_3Cit changed the zeta potential to more negative.

Table 4.3. Conductivity of process water with added chemicals

Conductivity	**NaOH**	**Na_3Cit**
mS/cm	mM	mM
2.728	0	0
3.102	0	1
3.329	5	0
3.700	5	1
3.921	10	0
4.312	10	1
5.315	15	0
5.672	15	1

The decreased change of magnitude of the mean zeta potential was due to the increased ionic strength. However, it could be seen that conductivity became even higher after Na_3Cit addition (Table 4.3). Higher conductivity indicated a higher ionic strength (Simón & García, 1999). This means that Na_3Cit shifted the zeta potential of real fines regardless of increased ionic strength.

In order to further prove that the synergistic effect was caused by Na_3Cit and not by the Na^+ ions, the zeta potential of real fines was also tested individually under two conditions: NaOH + Na_3Cit and NaOH + NaCl. The composition of process water used in the current experiments as well as the water chemistry is unknown, thus the ionic strength could not be calculated. However, the conductivity could be used to represent the ionic strength because it provides relevant information. If the conductivities of two solutions are the same, one might assume that the two solutions have roughly the same ionic strength. The conductivities of the process water after adding

different dosage of chemicals are shown in Table 4.4. It can be seen that the conductivities of co-addition of 15 mM NaOH and 1 mM Na_3Cit are roughly the same as the co-addition of 15 mM NaOH and 3 mM NaCl, suggesting similar ionic strength.

Table 4.4. Conductivity comparation after adding Na_3Cit and NaCl into process water

Conductivity	**NaOH**	**Na_3Cit**	**NaCl**
mS/cm	mM	mM	mM
5.623	15	1	0
5.560	15	0	3

The zeta potentials of three kinds of fines under two situations were compared, as shown in Figures 4.7 a–c. It was found that the zeta potential distributions of No. 18 fines with the co-addition of NaOH and Na_3Cit were more negative than that with the co-addition of NaOH and NaCl. Similar results for No. 23 fines and mixed fines could also be observed (Figures 4.7b and 4.7c). It was thereby concluded that the difference in zeta potential was not caused by the variation in ionic strength, but it was attributed to the addition of Na_3Cit. The co-addition of NaOH and NaCl simply changed zeta potential by depressing the electrical double layer, while the co-addition of NaOH and Na_3Cit changed zeta potential negatively by their synergistic effect.

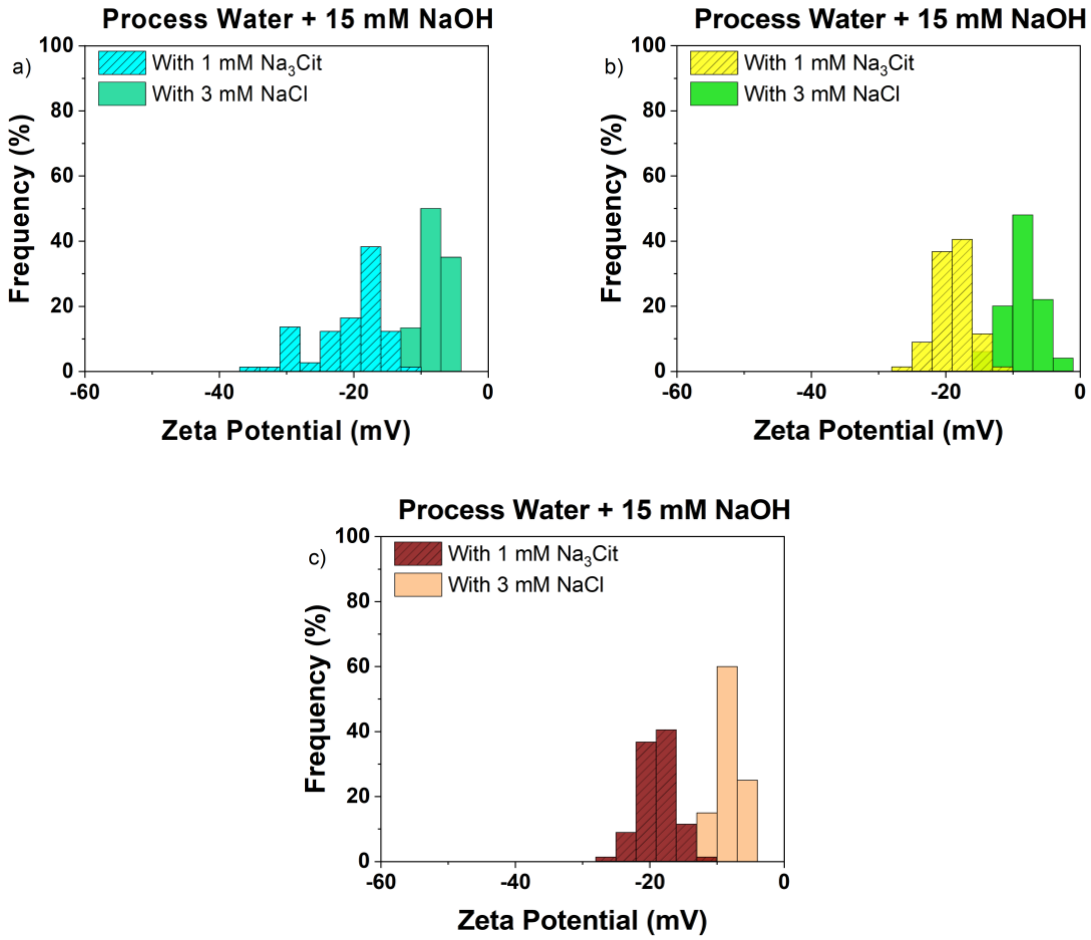

Figure 4.7. Zeta potentials of a) No. 18 fines, b) No. 23 fines, and c) mixed fines in the process water with co-addition of 15 mM NaOH + 1 mM Na_3Cit and co-addition of 15 mM NaOH + 3 mM NaCl.

4.3.3. Synergistic Effect of NaOH and Na_3Cit on the Zeta Potential of Bitumen

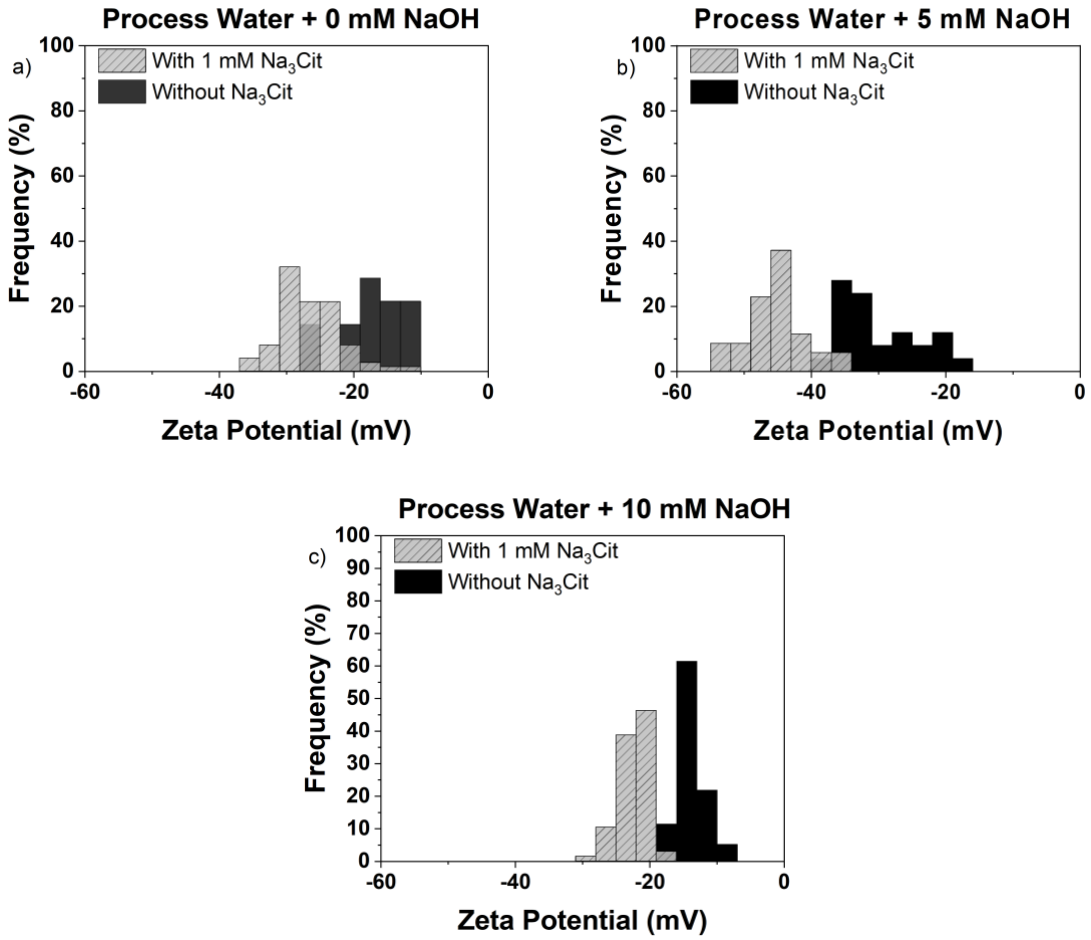

Figure 4.8. Effect of Na_3Cit and NaOH dosage on the zeta potential of bitumen in the process water from Plant 5. The concentration of NaOH changed from a) 0 mM to b) 5mM to c) 10 mM.

It can be seen from Figure 4.8a that adding 1 mM Na_3Cit shifted the distribution of zeta potential of bitumen to more negative. Besides, in the presence of 5 mM NaOH, the effect of Na_3Cit on changing the zeta potential of bitumen was more significant. Two distributions where 5 mM NaOH and 1 mM Na_3Cit were co-added and 5 mM NaOH alone was added were apart from each other, indicating the synergistic effect of NaOH and Na_3Cit (Figure 4.8b). However, with the

increasing dosage of NaOH to 10 mM, such synergistic effect became less significant as the two peaks of zeta potential distributions moved closer to each other (Figure 4.8c).

In general, results on the effect of NaOH and Na_3Cit on the individual colloidal particle types (fines or bitumen) showed that high dosage of NaOH made the zeta potential of fines less negative while the co-addition of NaOH and Na_3Cit negatively shifted zeta potential regardless of the increased ionic strength. Such results may help understand the role that Na_3Cit plays in preventing the slime coating of fines and bitumen.

4.3.4. Synergistic Effect of NaOH and Na_3Cit on the Slime Coating

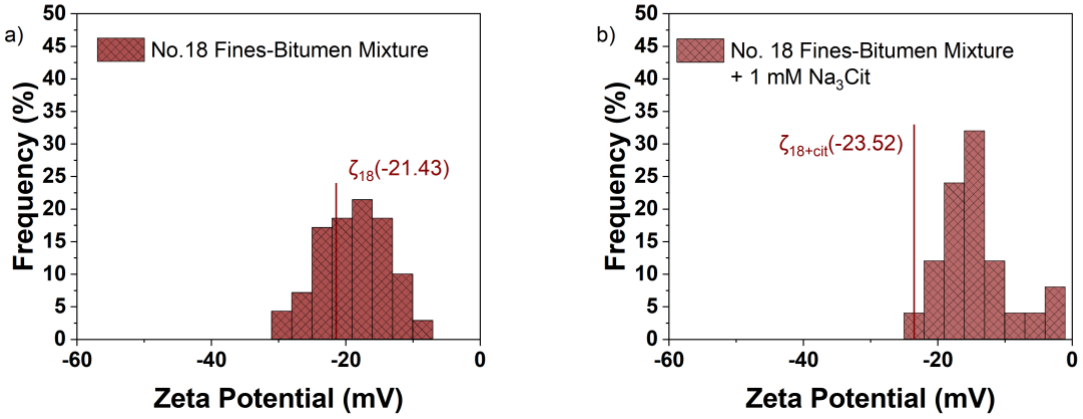

Figure 4.9. a) Interaction of No.18 Fines and bitumen in the process water without adding chemicals and b) with addition of 1 mM Na_3Cit.

As presented in Figure 4.9a, No. 18 fines and bitumen were mixed together. The resulted mixture showed one distribution, indicating the presence of slime coating between No.18 fines and bitumen. However, Figure 4.9b showed one single peak when adding 1 mM Na_3Cit before No. 18 fines and bitumen were mixed. There might have two reasons for this result. On one hand, Na_3Cit alone may not be able to prevent the hetero-coagulation of real fines and bitumen in the process water since it has been concluded that Na_3Cit and NaOH need to work synergistically on changing

the zeta potential of real fines. On the other hand, as shown in the previous results, zeta potential of No. 18 fines in the presence of process water containing 1 mM Na_3Cit overlapped with that of bitumen in the same water chemistry. Thus, the current result shown in Figure 4.9 might not be conclusive on explaining whether Na_3Cit alone could prevent slime coating of bitumen and real fines.

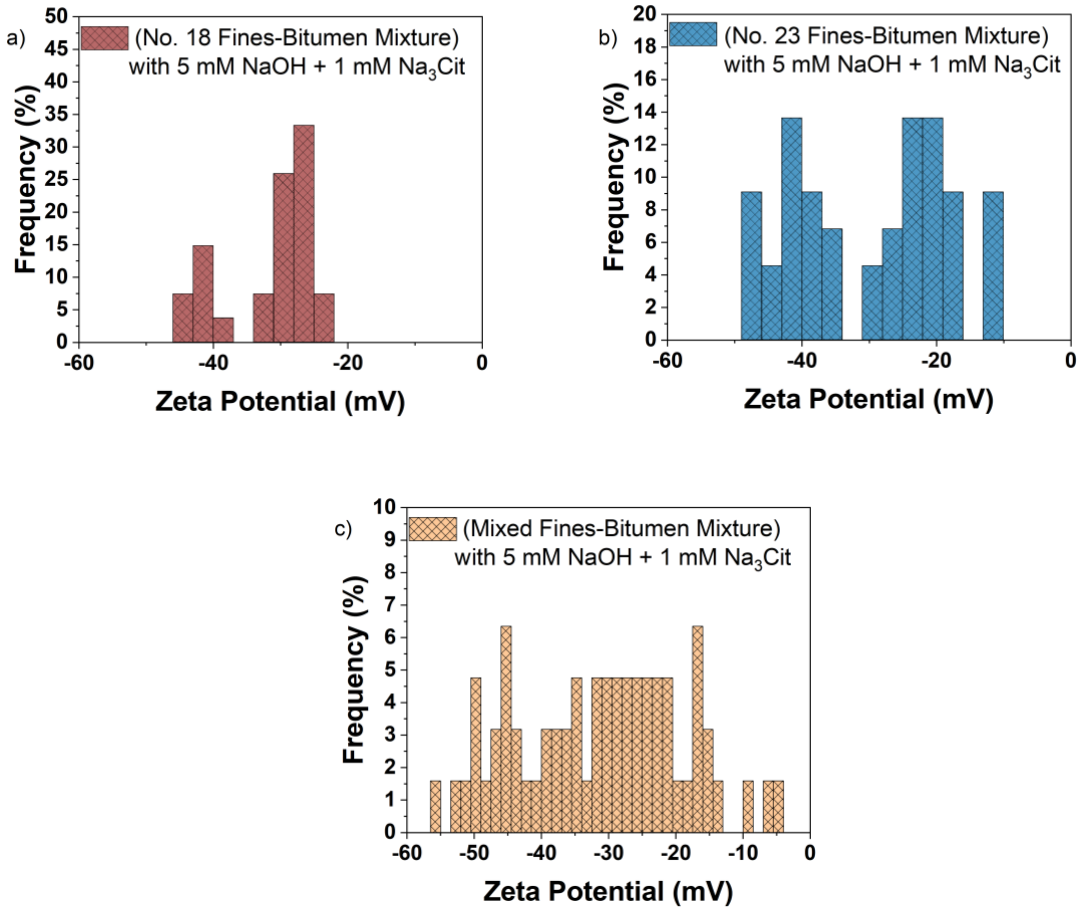

Figure 4.10. Zeta potential distributions of a) No. 18 fines-bitumen mixture b) No. 23 fines-bitumen mixture and c) No.53-No.58 mixed fines-bitumen mixture in the process water with co-added 1 mM Na_3Cit and 5 mM NaOH.

However, it could be conclusive that the co-addition of Na_3Cit and NaOH were able to prevent slime coating due to their synergistic effect. For the mixture of bitumen with three kinds of fines used in the current research, their zeta potentials showed distinct distributions when 5 mM NaOH and 1 mM Na_3Cit were added together in the process water (Figures 4.10a, b, and c).

4.4. Conclusions

In this chapter, the role of sodium citrate on slime coating was studied using bitumen-contanminated kaolinite and real oil sands fines. Experimental results showed that hydrophobilized kaolinite could cause slime coating whereas kaolinite could not. For the real fines extracted from oil sands, it was found that Na_3Cit alone did not change the zeta potential a lot but the combination of NaOH and Na_3Cit could make the zeta potential more negative. When it comes to the mixture of bitumen and real fines, the co-addition of NaOH and Na_3Cit played synergistic role on preventing the slime coating of bitumen by real fines.

Chapter 5 Conclusion and Future work

5.1. Conclusion

In this study, three techniques have been used to investigate the effect of sodium citrate on the interactions between bitumen and different clays in process water. Synergistic effect of sodium hydroxide and sodium citrate was shown to be beneficial on preventing slime coating from happening.

Zeta potential was first used to study the effect of sodium citrate on the interaction between bitumen and clays such as kaolinite, illite, and montmorillonite. The addition of sodium citrate made the zeta potential of bitumen and all individual clays more negative in the process water from Aurora Plant. By zeta potential distribution measurements, it was found that montmorillonite caused slime coating of bitumen while neither kaolinite nor illite induced slime coating. The addition of sodium citrate before montmorillonite suspension and bitumen emulsion were mixed resulted in the separated zeta potential distributions, indicating that sodium citrate was able to effectively prevent bitumen from slime coating of montmorillonite.

QCM-D technique was then used to verify and confirm the results obtained by zeta potential measurements. By monitoring frequency and dissipation changes of bitumen coated sensor with QCM-D, it was found that both frequency and dissipation experienced huge change after montmorillonite suspension was pumped into the chamber. When process water containing sodium citrate was introduced, much less changes of both frequency and dissipation were observed. There was no noticeable change after kaolinite or illite suspension was introduced, indicating no adsorption of kaolinite or illite onto the bitumen-water interface. Therefore, zeta potential results and QCM-D results were consistent in supporting the slime coatings observed in this research.

In order to make convincing and straightforward conclusions, SEM-EDS technique was used to show the morphology and element composition of montmorillonite slime. First, SEM images of two bitumen coated sensors onto which montmorillonite suspensions were introduced with or without sodium citrate showed the effect of sodium citrate. Second, the characteristic feature of curl and lamellar confirmed that the white particles on the sensor were clays. EDS spectrum clearly showed the peaks of Al and Si, dominating elements in the clay, and peak of Fe, which comes from isomorphic substitution.

To bridge the gap between ideal and real industrial systems, three kinds of real fines were used to study the effect of sodium citrate alone and the synergistic effect of sodium citrate and sodium hydroxide. It was found that the zeta potentials of all three fines did not change in the presence of sodium citrate alone. Sodium hydroxide was able to change the zeta potential of all of three fines to more negative at low dosage but decreased the magnitude of the zeta potential at high dosage, due to the depression of the electrical double layer. Compared with the zeta potential of real fines in the presence of high dosage of sodium hydroxide, the zeta potential distribution after co-addition of sodium hydroxide and sodium citrate was more negative, indicating their synergistic effect. Increasing in the magnitude of the zeta potential leads to higher repulsion between bitumen and fines, which is the synergistic role of sodium hydroxide and sodium citrate.

In conclusion, sodium citrate alone could change the zeta potential of clays to more negative and prevent hetero-coagulation of bitumen and clays. However, sodium citrate alone did not change the zeta potential of real fines. The synergistic effect of sodium citrate and sodium hydroxide not only shifted the zeta potential of real fines to more negative, but also prevented the slime coating of bitumen from real fines.

5.2. Future Work

QCM-D technique could be used to study the adsorption of fines onto bitumen-water interface with the co-addition of sodium hydroxide and sodium citrate. However, at the high dosage of sodium hydroxide, the undesired unstable bitumen film on the QCM-D sensor may give inaccurate results.

Force measurements by atomic force microscopy (AFM) between bitumen and different fine particles such as kaolinite, illite, montmorillonite, and real fines in the presence of sodium citrate and sodium hydroxide are of importance. They could reveal the synergistic effect of sodium hydroxide and sodium citrate on the interaction forces between bitumen and clays.

References

Arnold, B. J., & Aplan, F. F. (1986). The effect of clay slimes on coal flotation, part I: The nature of the clay. *International Journal of Mineral Processing*, 17(3-4), 225-242.

Benco, L., Tunega, D., Hafner, J., & Lischka, H. (2001). Upper Limit of the O− H⊙⊙⊙ O Hydrogen Bond. Ab Initio Study of the Kaolinite Structure. *The Journal of Physical Chemistry B*, 105(44), 10812-10817.

Bergaya, F., & Lagaly, G. (2013). *Handbook of clay science*. Newnes.

Chang, J., Liu, B., Grundy, J. S., Shao, H., Manica, R., Li, Z., ... & Xu, Z. (2021). Probing Specific Adsorption of Electrolytes at Kaolinite–Aqueous Interfaces by Atomic Force Microscopy. *The Journal of Physical Chemistry Letters*, 12(9), 2406-2412.

Chen, Q., Xu, S., Liu, Q., Masliyah, J., & Xu, Z. (2016). QCM-D study of nanoparticle interactions. *Advances in Colloid and Interface Science*, 233, 94-114.

Clark, K. A., & Pasternack, D. S. (1932). Hot Water Seperation of Bitumen from Alberta Bituminous Sand. *Industrial and Engineering Chemistry*, 24(12), 1410–1416.

Deng, M., Liu, Q., & Xu, Z. (2013). Impact of gypsum supersaturated solution on surface properties of silica and sphalerite minerals. *Minerals Engineering*, 46, 6-15.

Ding, X., Repka, C., Xu, Z., & Masliyah, J. (2008). Effect of Illite Clay and Divalent Cations on Bitumen Recovery. *The Canadian Journal of Chemical Engineering*, 84(6), 643–650.

Doymuş, K. (2007). The effect of ionic electrolytes and pH on the zeta potential of fine coal particles. *Turkish Journal of Chemistry*, 31(6), 589–597.

Edwards, C. R., Kipkie, W. B., & Agar, G. E. (1980). The effect of slime coatings of the serpentine minerals, chrysotile and lizardite, on pentlandite flotation. *International Journal of Mineral Processing*, 7, 413–420.

Flury, C., Afacan, A., Tamiz Bakhtiari, M., Sjoblom, J., & Xu, Z. (2014). Effect of caustic type on bitumen extraction from Canadian oil sands. *Energy & fuels*, 28(1), 431-438.

Forbes, E., Davey, K. J., & Smith, L. (2014). Decoupling rehology and slime coatings effect on the natural flotability of chalcopyrite in a clay-rich flotation pulp. *Minerals Engineering*, 56, 136–144.

Gan, W., & Liu, Q. (2008). Coagulation of bitumen with kaolinite in aqueous solutions containing Ca2+, Mg2+ and Fe3+: Effect of citric acid. *Journal of colloid and interface science*, 324(1-2), 85-91.

Gee, M. L., Healy, T. W., & White, L. R. (1990). Hydrophobicity effects in the condensation of water films on quartz. *Journal of colloid and interface science*, 140(2), 450–465.

Gu, G., Sanders, R. S., Nandakumar, K., Xu, Z., & Masliyah, J. H. (2004). A novel experimental technique to study single bubble-bitumen attachment in flotation. *International Journal of Mineral Processing*, 74(1–4), 15–29.

Gu, G., Xu, Z., Nandakumar, K., & Masliyah, J. (2003). Effects of physical environment on induction time of air-bitumen attachment. *International Journal of Mineral Processing*, 69(1–4), 235–250.

Hunter, R. J. (1981). The Calculation of Zeta Potential. Zeta Potential in Colloid Science, 59–124.

Kasongo, T., Zhou, Z., Xu, Z., & Masliyah, J. (2000). Effect of clays and calcium ions on bitumen extraction from Athabasca oil sands using flotation. *The Canadian Journal of Chemical Engineering*, 78(4), 674–681.

Lin, F., Nolan, L., Xu, Z., & Cadien, K. (2012). A Study of the Colloidal Stability of Mixed Abrasive Slurries and Their Role in CMP. *Journal of The Electrochemical Society*, 159(5), H482–H489.

Liu, J., Vandenberghe, J., Masliyah, J. H., Xu, Z., & Yordan, J. L. (2007). Fundamental study on talc-ink adhesion for talc-assisted flotation deinking of wastepaper. *Minerals Engineering*, 20(6), 566–573.

Liu, J., Xu, Z., & Masliyah, J. (2003). Studies on bitumen− silica interaction in aqueous solutions by atomic force microscopy. *Langmuir*, 19(9), 3911-3920.

Liu, J., Xu, Z., & Masliyah, J. (2004). Interaction between bitumen and fines in oil sands extraction system: Implication to bitumen recovery. *The Canadian Journal of Chemical Engineering*, 82(4), 655-666.

Liu, J., Xu, Z., & Masliyah, J. (2004). Role of fine clays in bitumen extraction from oil sands. *AIChE journal*, 50(8), 1917-1927.

Liu, J., Xu, Z., & Masliyah, J. (2005). Interaction forces in bitumen extraction from oil sands. *Journal of colloid and interface science*, 287(2), 507–520.

Liu, J., Zhou, Z. A., Xu, Z., & Masliyah, J. H. (2002). Bitumen-clay interactions in aqueous media studied by zeta potential distribution measurement. *Journal of colloid and interface science*, 252(2), 409–418.

Long, J., Drelich, J., Xu, Z., & Masliyah, J. H. (2007). Effect of operating temperature on water-based oil sands processing. *The Canadian Journal of Chemical Engineering*, 85(5), 726–738.

Long, J., Xu, Z., & Masliyah, J. H. (2006). Role of illite-illite interactions in oil sands processing. *Colloids and Surfaces A: Physicochemical and Engineering Aspects*, 281(1–3), 202–214.

Madge, D. N., Romero, J., & Strand, W. L. (2004). Hydrocarbon cyclones in hydrophilic oil sand environments. *Minerals Engineering*, 17(5), 625–636.

Masliyah, J. H., Czarnecki, J., & Xu, Z. (2011). Handbook on Theory and Practice on Bitumen Recovery from Athabasca Oil Sands.

Masliyah, J., Zhou, Z. J., Xu, Z., Czarnecki, J., & Hamza, H. (2004). Understanding water-based bitumen extraction from Athabasca oil sands. *The Canadian Journal of Chemical Engineering*, 82(4), 628-654.

Mignon, P., Ugliengo, P., Sodupe, M., & Hernandez, E. R. (2010). Ab initio molecular dynamics study of the hydration of Li+, Na+ and K+ in a montmorillonite model. Influence of isomorphic substitution. *Physical Chemistry Chemical Physics*, 12(3), 688-697.

Miller, J. D., & Misra, M. (1982). Hot water process development for Utah tar sands. *Fuel Processing Technology*, 6(1), 27-59.

Misra, M., & Miller, J. D. (1991). Comparison of water-based physical separation processes for US tar sands. *Fuel processing technology*, 27(1), 3-20.

Oats, W. J., Ozdemir, O., & Nguyen, A. V. (2010). Effect of mechanical and chemical clay removals by hydrocyclone and dispersants on coal flotation. *Minerals Engineering*, 23(5), 413–419.

Pauling, L. (1930). The structures of the micas and related minerals. *Proceedings of the National Academy of Sciences of the United States of America*, 16, 123–129.

Rabiller-Baudry, M., & Chaufer, B. (2001). Specific adsorption of phosphate ions on proteins evidenced by capillary electrophoresis and reversed-phase high-performance liquid chromatography. *Journal of Chromatography B: Biomedical Sciences and Applications*, 753(1), 67-77.

Reddi, L., & Inyang, H. I. (2000). *Geoenvironmental engineering: principles and applications.* CRC Press.

Sepulveda, J. E., & Miller, J. D. (1978). Extraction of bitumen from Utah tar sands by a hot water digestion-flotation technique. *Soc. Pet. Eng. AIME, Pap.;(United States)* , 78(CONF-780213-).

Schoonheydt, R. A., & Johnston, C. T. (2006). Surface and interface chemistry of clay minerals. *Developments in clay science*, 1, 87-113.

Schoonheydt, R. A., Johnston, C. T., & Bergaya, F. (2018). Clay minerals and their surfaces. In *Developments in Clay Science* (Vol. 9, pp. 1-21). Elsevier.

Schramm, L. L., Mannhardt, K., & Novosad, J. J. (1991). Electrokinetic properties of reservoir rock particles. *Colloids and surfaces*, 55, 309-331.

Simón, M., & García, I. (1999). Physico-chemical properties of the soil-saturation extracts: Estimation from electrical conductivity. *Geoderma*, 90(1–2), 99–109.

Sposito, G. (2019). Characterization of particle surface charge. In *Environmental particles* (pp. 291-314). CRC Press.

Takamura, K. (1982). Microscopic structure of Athabasca oil sand. *The Canadian Journal of Chemical Engineering*, 60(4), 538-545.

Tamiz Bakhtiari, M., Harbottle, D., Curran, M., Ng, S., Spence, J., Siy, R., … Xu, Z. (2015). Role of caustic addition in bitumen-clay interactions. *Energy & Fuels*, 29(1), 58–69.

Tournassat, C., Bourg, I. C., Steefel, C. I., & Bergaya, F. (2015). Surface properties of clay minerals. In *Developments in clay science* (Vol. 6, pp. 5-31). Elsevier.

Wang, B., Peng, Y., & Vink, S. (2013). Diagnosis of the surface chemistry effects on fine coal flotation using saline water. *Energy & Fuels*, 27(8), 4869–4874.

Wu, C., Wang, L., Harbottle, D., Masliyah, J., & Xu, Z. (2015). Studying bubble-particle interactions by zeta potential distribution analysis. *Journal of colloid and interface science*, 449, 399–408.

Xiang, B., Li, R., Liu, B., Manica, R., & Liu, Q. (2020). Effect of Sodium Citrate and Calcium Ions on the Spontaneous Displacement of Heavy Oil from Quartz Surfaces. *The Journal of Physical Chemistry C*, 124(38), 20991-20997.

Xiang, B., Liu, Q., & Long, J. (2018). Probing Bitumen Liberation by a Quartz Crystal Microbalance with Dissipation. *Energy & Fuels*, 32(7), 7451–7457.

Xiang, B., Truong, N. T. V., Feng, L., Bai, T., Qi, C., & Liu, Q. (2019). Study of the Role of Sodium Citrate in Bitumen Liberation. *Energy & Fuels*, 33(9), 8271–8278.

Yan, N., & Masliyah, J. H. (1994). Adsorption and Desorption of Clay Particles at the Oil-Water Interface. *Journal of colloid and interface science*, 168(2), 386-392.

Yu, Y., Ma, L., Cao, M., & Liu, Q. (2017). Slime coatings in froth flotation: A review. *Minerals Engineering*, 114, 26-36.

Zhang, D. (2020). Effects of Sodium Citrate on Slime Coatings in Bitumen Extraction.

Zhao, H., Long, J., Masliyah, J. H., & Xu, Z. (2006). Effect of divalent cations and surfactants on silica-bitumen interactions. *Industrial and Engineering Chemistry Research*, 45(22), 7482–7490.

Appendix A X-ray Diffraction Analysis for Clay

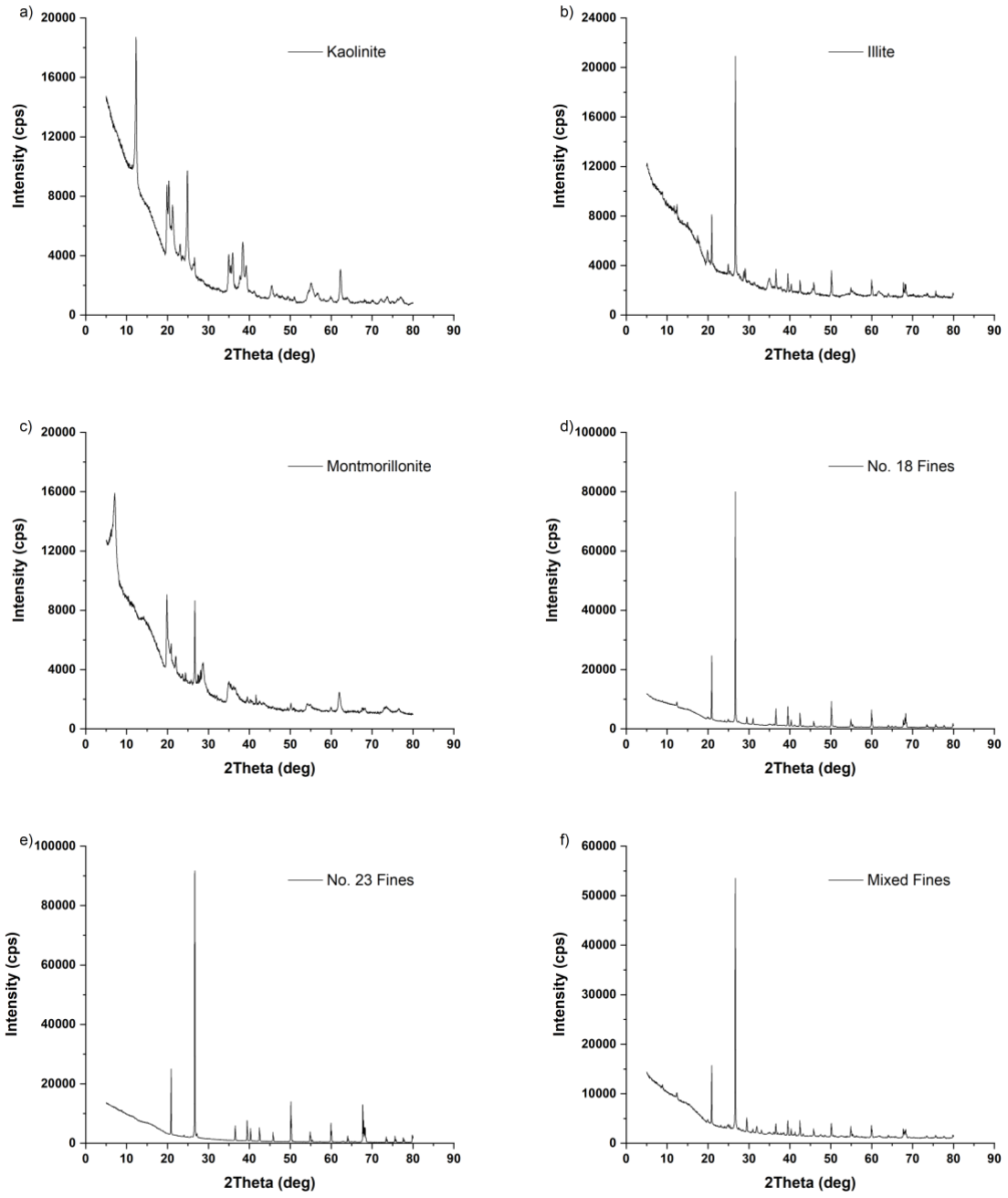

Figure A.1. XRD analysis of a) kaolinite, b) illite, c) montmorillonite, d) No. 18 fines, e) No. 23 fine, and f) mixed fines in current research.